MAX-PLANCK-INSTITUT FÜR PLASMAPHYSIK

GARCHING BEI MÜNCHEN

TIME-RESOLVING COLLECTOR PROBES

Basic Investigations, Design and Construction

J. Ehrenberg, P. Børgesen and C. Dorn

IPP 9/49 September 1984

The content of this report
was previously published in IPP-JET No. 24

Die nachstehende Arbeit wurde im Rahmen des Vertrages zwischen dem Max-Planck-Institut für Plasmaphysik und der Europäischen Atomgemeinschaft über die Zusammenarbeit auf dem Gebiete der Plasmaphysik durchgeführt.

IPP 9/49

J. Ehrenberg
P. Børgesen
C. Dorn

Time-Resolving Collector Probes
Basic Investigations, Design
and Construction

(in English)

Abstract

For the Plasma Boundary Probe System and the Fast Transfer System at JET the design of a Time Resolving Collector Probe was performed. Special attention was given to the collector material and its implication to the analysis technique used to detect the deposited fluxes of hydrogen and impurities after plasma exposure.

The investigations on the collector material showed that widely used Papyex is inadequate due to high level bulk impurities (some 100 ppm). Instead, well purified graphite, even in the dimensions needed is available and can be obtained with a rather smooth surface (roughness < 2 um). Routine analysis of collector probe surfaces with regard to impurity fluxes after having been exposed to the plasma can be performed most conveniently by means of Proton Induced X-Ray Analysis (PIXE) or Rutherford Backscattering Spectrometry (RBS). PIXE has the advantage of discriminating the elements in question better than RBS (stainless steel components for instance) whereas RBS gives some depth discrimination. The value of this, however, is in doubt because of possible metal droplet formation on the collector surface. The mechanical layout of the probe enables a fast exchange of single components without changing others. This allows the use of different collector materials lateron (for instance Silicon) and assures a more flexible use of the probe for different purposes (H trapping and depth profiling).

C O N T E N T S

I) Introduction

II) Scope of the work

III) Basic investigations
III.1) Requirements for time resolving collector probes
III.1.1) Requirements for collection
III.1.2) Requirements specific to the analysis technique
III.1.3) Requirements for handling
III.2) Experiments
III.3) Results
III.3.1) Temperature dependence of impurity concentrations
III.3.2) Thermal behaviour of a Ni film on graphite and silicon samples
III.3.3) Exposure to plasma discharges
III.4) Discussion
III.4.1) Impurities
III.4.2) Metal layers
III.4.3) Analysis of probe surface after plasma exposure
III.5) Conclusions

IV) Design and construction of the probe
IV.1) Probe interface
IV.2) Probe shield
IV.3) Probe collector
IV.5) Materials

V) References

VI) Figure Captions

VII) List of Tables

VIII) Captions of probe and component drawings

I) INTRODUCTION

Among other diagnostic methods, plasma wall interaction studies in JET will also be performed by means of time-resolving collector probe measurements (T R C P). In principle TRCP's consist of a solid surface which is exposed to the plasma boundary layer and is rotated behind an aperture during a discharge to give a time discrimination of collected particle fluxes. After the discharge the probe is removed from the plasma and introduced into a surface analysis chamber where the deposited material is is investigated.
AT JET three systems will be provided to perform such measurements:

1) The Plasma Boundary Probe System (PBPS) /1/
2) The Fast Transfer System (FTS) /1/
3) The Surface Analysis Station (SAS) /1/

1) and 2) are the systems used for introducing the probes into the plasma boundary layer whereas 3) will be used for analysis of the deposits on the probe surface. FTS and SAS are connected via a probe trolley to each other allowing in situ analysis of exposed probes whereas probes from system 1 will be attached at the SAS via a vacuum suitcase.
For the scientific and engineering design and construction of probes described in this report an article 14 contract was placed between JET and IPP.

II) SCOPE OF THE WORK

The work was divided in two parts:

1) Investigations of collector materials. These works considered the suitability of materials with regard to the collection of atoms in the plasma as well as to the methods of analysis provided in the SAS. Suggestions about suitable materials are given.
2) Design and construction of the probe.
This part is concerned with the shape and mechanical details of the probe, with special attention to the probe interface where the manipulator of FTS, PBPS and SAS have to grip the probe. The work was performed in close collaboration with JET, Culham Laboratories (Design of FTS) and Pfeiffer/Asslar (FRG) (Construction of PBPS and SAS). A complete set of manufactory drawings is given and material suggestions are made.

III) BASIC INVESTIGATIONS

III.1) Requirements for time resolving collector probes

The main parameters usually measured in collector probe experiments are deposited fluxes of hydrogen or wall atoms, so called impurities, in the plasma boundary layer or at wall sites. The collector material must therefore fulfill predominantly three types of requirements:

III.1.1) Requirements for collection:

Initial impurity concentrations at the surface have to be sufficiently low to ensure low detection limits. Segregation of bulk impurities to the surface should be negligible. Sticking probability for plasma impurities and hydrogen and thermal behaviour of collected atoms on the surface of the material should be known. Good thermal behaviour of the collector material (high melting point, good heat conduction) is also needed.

III.1.2) Requirements specific to the analysis technique:

Rutherford Backscattering Spectroscopy (RBS) and Proton Induced X-Ray Emission (PIXE) have proven particularly suitable for fast routine analysis of many samples /Bø 84/. Other analysis methods, such as AES, SIMS, EIXE etc. are also used /St 78, McCr 79, Zu 84/ but lack the quantitative precision of the ion beam methods.

In the following, we shall confine ourselves to RBS and PIXE analysis which will be the main analysis techniques in the SAS. For fast routine measurements high current ion beams are used and thus low Z collector materials are needed in order to avoid pulse pile up in the detectors. For the case of RBS one should furthermore prefer very low Z collector materials in order to measure low Z deposits such as oxygen.
Compared to RBS, PIXE is sensitive to larger depths. This may be needed when rough collector surfaces are analysed or thermal processes have distributed the collected atoms into the bulk. Quantitative results can be obtained by calibration.

III.1.3) Requirements for handling

A final requirement for the applicability of a collector material is its practical handling and its machinability. This may often be important because of the particular probe geometries needed.
In the past, several materials such as graphite, silicon, aluminium and beryllium have been used for collector probes /Ta 82, Wi 82, Ho 82/. Graphite has the advantage of low Z and good thermal properties, but suffers sometimes from bulk impurities /Bø 84/. Nevertheless it is one of the most frequently used collector materials. We investigated the following graphites in view of their suitability for collector probes in plasma experiments:

(i) Vitreous graphite, where a very smooth surface can be obtained (necessary for depth profiling).

(ii) Pyrolytic graphite, similar to a graphite single crystal, available to quite high purity.

(iii) Papyex, a flexible graphite foil, very practical in handling and mounting, not very pure, often used as collector material.

(iv) Poco graphite, fine grain graphite, therefore easily machinable, but high porosity.

(v) Silicon, as reference material, very pure.

III.2) Experiments

The materials listed above were investigated with respect to the following properties:

(i) Purity of the sample and its dependence on temperature.

(ii) Thermal behaviour of metal films on the sample surface.

(iii) Erosion of vapour deposited metal layers during plasma discharges.

For analysis RBS/Ch 78/ and PIXE /Jo 76/ were used and a comparison of these methods was made with respect to routine analysis measurements of collector probes. For RBS we used a 1 MeV $^{4}He^{+}$ beam and a backscattering angle of 165°. PIXE measurements were made with a 1.5 MeV proton beam and a detector angle of 135°. Supplementary analysis was made with a scanning electron microscope /St 77/ which allowed in situ Electron Induced X-ray Emission analysis (EIXE).

During heating experiments RBS measurements were performed in situ ($p \sim 10^{-7}$ mbar) whereas the samples had to be exposed to air before PIXE analysis.
The heating procedures consist of a nearly linear temperature rise within a few minutes up to a temperature T which was then held for about 5 minutes and a subsequent cooling down to room temperature.

The thermal behaviour of a layer with 1×10^{17} Nickel atoms/cm^2 (100 Å) was studied for each of the above substrates.

For the measurements of erosion and deposition during plasma discharges 3.5×10^{16} Pd-atoms/cm^2 were evaporated onto a Papyex stripe which was then mounted on a collector probe /Ta 82/ and exposed in the upper divertor chamber of ASDEX. Pd was chosen as an element usually not present in the plasma, allowing simpler interpretation of concentration variations. Additionally, these measurements were used for a comparison between PIXE and RBS analysis of collector probe surfaces.

III.3) Results

III.3.1) Temperature dependence of impurity concentrations.

Figure 1 a, b, c) shows RBS-spectra of the virgin graphite samples after heating from 300 K a), to 840 K b), and to 930 K c). Generally a reduction of impurity concentration is observed. Vitreous graphite shows high impurity concentrations at masses below Ca and only few signals from higher masses whereas the other graphite samples are purer but contain additional high mass elements.Silicon is not shown here as essential no impurities could be detected with the present methods. The variation with temperature of impurity concentrations in the surface layer ($\lesssim$ 1000 Å) seen with RBS is also observed in the bulk by PIXE measurements (Fig. 2a, b) for T = 300 K and T = 930 K.

Table 1 gives an overview of the quantities measured. Peaks in the RBS spectra were evaluated as surface concentrations (atoms/cm^2) whereas broader signals (steps) were evaluated as bulk concentrations (atoms/carbon atom).
Quantities obtained with PIXE were evaluated in both ways, i.e. as surface and as bulk concentratrions, as these may not be distinguished in a PIXE spectrum. Differences between RBS and PIXE results might be due to very inhomogeneous concentration distributions along the sample surface. Concentrations were observed to vary by factors of up to ten over short distances /BØ 84/. Common to all graphite samples is a high content of oxygen (about 10^{15} O-atoms/cm^2). This can be reduced, by heating, to quantities not exceeding the overall background signals.

III.3.2) Thermal behaviour of a Ni film on graphite and on silicon samples

The modification of a Ni layer on Papyex and silicon with temperature is given in Fig. 3a, b). The other graphite samples behaved similarly. The heating procedure was carried out to 620 K, 830 K, and 1090 K. For the first two temperatures no variations of the RBS spectra were seen. At 1090 K a broadening of the Ni signal and a shift of the substrate backscattering edge toward higher energies is observed. The Ni peak broadening varied somewhat from sample to sample, probably due to different thermal contact. Both, with RBS and PIXE the total amount of Ni was seen to remain constant within the experimental uncertainties ($\pm$ 10 %). Table 2 gives the quantitative results for nickel and oxygen measured by RBS and for the main impurities measured by PIXE. In contrast to the behaviour without Ni-coverage (Fig.1) the large oxygen concentration (3 - 10 x 10^{16} at/cm^2) was now hardly reduced by heating, suggesting the presence of an oxide. In general, the impurity contents were not reduced by heating (compare Figs. 1, 2).

Figure 4 shows the surface structure of the graphite and silicon samples with the Ni film after heating to 1090 K. Agglomeration of Ni into droplets can be clearly seen independent of the surface topography. EIXE-spectra measured with a strongly focussed electron beam (fig.5 and 6) show that a droplet typically contains more than 1.5 x 10^{17} Ni atoms/cm^2, whereas there were less than 10^{16} Ni atoms/cm^2 between droplets. This should be compared to an original film thickness of 1 x 10^{17} Ni atoms/cm^2 (see above).

III.3.3) Exposure to plasma discharges

The results of our probe measurements in plasma discharges can be roughly divided into two parts. Those measurements where no visible surface damage of the collector surface occurred and those where the surface is severely damaged by high heat loads. First we will consider the former.
Figure 7a, b) gives the result of a time resolved collector measurement analysed with RBS and PIXE. In Fig. 7c) the variations of plasma parameters during the discharge are shown.

Within our experimental errors no erosion of Pd can be detected, i.e. an upper erosion limit of 3×10^{15} Pd/cm^{2}s can be given corresponding to the statistical uncertainties of the measurement.The RBS analysis shows concentration profiles of Fe, O and S which are closely related to each other.(Elements between Ti and Fe are not discriminated by 1 MeV He RBS). For Fe and O they are clearly above the conficence limits for these elements in Papyex (for Fe: 1.5×10^{14} at/cm^2; for O: 4×10^{15} at/cm^2) /BØ 84/. The confidence limit for sulphur(1×10^{15} atoms/cm^2)/ BØ 84/ is nearly as large as the peak concentration.

Figure 7b) shows the results of the PIXE measurements. Within the time resolution of the exposure the profiles of the metallic components are quite similar to the Fe distribution given in Fig. 7a). Particularly the time distribution of Ti is very similar to the RBS results, whereas the stainless steel components are shifted towards later times. They do, however, have nearly identical profiles. The sum of the maximum amounts of Fe, Cr, Ni, measured with PIXE is about 2×10^{16} at/cm^2. Subtraction of the background (confidence limit) of each of the elements /BØ 84/ give an integral amount of about 9×10^{15} at/cm^2. This is a factor of 10 more than seen in the RBS peak. The reason for this discrepancy is discussed later.
The results for a time integrated measurement (without rotation of the collector) during one discharge are shown in figs. 8a, b. This

is an example where surface damage of the Papyex is observed within the diameter of the aperture in front of the probe surface (compare the SEM viewgraphs of Fig.9). Several layers of Papyex were destroyed. The erosion of Pd is clearly detected, by both RBS and PIXE. Again, we observe a significant difference in the quantities of Fe measured by RBS and PIXE, as well as a difference in the Fe profiles. Severely damaged regions have also been observed during time resolved probe measurements.

III.4) DISCUSSION

III.4.1) Impurities

The purest material investigated here is silicon, which is furthermore available with a very smooth surface and as a single crystal allowing reliable depth profiling and the application of channeling. On the other hand, with RBS oxygen cannot be measured very sensitively on Si, and in general pulse pile up is a limitation in routine measurements /Bø 84/. Finally silicon is very brittle and cannot be handled and shaped very easily. Therefore it seems not to be suitable for routine plasma measurements but may have advantages for special cases as for hydrogen collection and depth analysis.

On graphite smooth surfaces can be realized by using vitreous graphite but this suffers from a lot of bulk impurities. Pyrolytic graphite is available to very high purities (< 0.1 ppm). The tightly closed surface minimizes effects of contamination with gases. Unfortunately the material is only available in rather thin platelets and coatings.

Poco graphite on the other hand is very easily machinable but very porous. A solution might be to use Poco graphite samples coated with a thin layer of pyrolytic graphite thus ensuring a closed surface.

The results in Table 1 show that without some additional cleaning (done mostly by heating) the oxygen background is a severe problem for determining collected fluxes of oxygen in plasma discharges. This problem is increased if metal atoms are simultaneously deposited on the probe surface (see III.4.3)
The presence of S, Cl, K, Ca and especially of Fe increases the difficulties in relating measured quantities to collected fluxes of deposited material. Segregation of these elements to the surface and a subsequent increase in surface concentration might occur when the probe is heated during exposure and when a metal layer of deposits on the surface works as a segregation barrier. This can only be reduced or avoided by the use of a very pure graphite (see III.4.)

III.4.2) Metal layers

The heating experiments showed a broadening of the RBS signal from a Nickel layer which was probably caused by metal agglomeration. The formation of droplets was observed independently of the surface topography of the samples. Similar formation of droplets also has been seen on limiter-surfaces of tokamaks after long term exposure /St 78, GL 80, Be 84/. The analysis of such surfaces required the use of PIXE, as the size of droplets exceeds the depth which can be quantitatively measured by RBS. PIXE measurements, on the other hand, demand a high bulk purity in graphite to avoid errors in the interpretation of deposited metal quantities. If droplets are formed depth profiles of metal deposits are no longer meaningful.

III.4.3) Analysis of probe surfaces after plasma exposure

In view of the results of section III.3.3) (Figs. 7 ,8) the apparent discrepancy between RBS and PIXE analysis of the stainless steel components might be explained as follows:
The metals are either distributed within the graphite bulk or/and exist in a few but large (µm) droplets on the surface. As PIXE is more sensitive to larger depths (>>1000 Å) than RBS, in both

cases one would still obtain a sizeable PIXE signal whereas RBS only gives a signal corresponding to the relative areal density of the metal near the surface.
For sulfur the difference between the measured profiles is easily understood. The RBS analysis shows a concentration variation near the surface (some 10^{14} S-atom/cm^2) which is too small to be discriminated from the background concentration seen with PIXE (see tables 1), 2)). Hence no similar profile as with RBS can be detected.
For an interpretation of collector measurements it must be somehow known whether the measured concentrations were deposited by the plasma or whether other processes, such as segregation, oxidation or previous contamination may contribute to the measured distributions. In our experiment, Pd could have formed a segregation barrier for sulfur, but even in experiments with very pure surfaces the deposition of material during the plasma exposure might create such a barrier.
In principle, segregation of metallic impurities is also possible. Comparison of the data in table 1) and 2) and the spectra in figs. 1) and 2) show the mobility of the impurities when the sample is heated.
Additionally, however, diffusion of metal into the graphite might also occur, which would also alter the concentration distribution in near surface regions. Thus RBS, which is sensitive in near surface regions, may measure profiles which are not only due to deposition but also influenced by segregation and/or diffusion. These difficulties can only be partially overcome by the use of PIXE, as the detection of concentration variations of some 10^{14} to 10^{15} atoms/cm^2 demands pure graphite samples with low enough background concentration of the elements in question. Clearly this would also reduce the difficulties for RBS.
An illustration of the advantage of very pure ($<$ ppm) collectors are the results of Pd (Figs. 7, 8) measured with PIXE and RBS, which are within the experimental errors identical. Pd is not a bulk impurity of Papyex. Unfortunately, however, typical plasma impurities as O and Fe are found in virgin Papyex.

Another and somewhat outstanding difficulty of probe measurements arises with relating measured oxygen quantities to deposited fluxes. Besides deposition, diffusion and segregation (Tables 1,2) the formation of oxides after plasma exposure and during storage or transfer of probes through air to the analysis chamber may increase the O concentration. This can only be avoided with in situ analysis of exposed probes under UHV conditions. However, these conditions are generally not present in plasma machines. At any rate one needs to use O free graphite ($\leq 10^{13}$ at/cm^2) in order to minimize and control influences on the measurements.

Besides the problems of determining deposited fluxes, erosion processes which occur simultaneously with deposition increase the difficulties to convert these to incident fluxes. The erosion of Pd given in Fig. 8) is due to a high heat load, as seen in Fig. 9). High heat loads may occur during some fraction of the discharge time and are often detected as burned spots on Papyex, when this material is used as collector. The use of other graphites as collector material may shift this problem to higher heat loads, but would not prevent erosion and evaporation of deposited material. Tests on the thermal behaviour of Papyex have shown the particular disadvantage of this material for collector probes. The variation of surface structure of Papyex depends on the speed of temperature rise. Slow rise as in our heating experiments does not alter the surface while a quick rise (500 K/s) gives bubble formation near 400^{0} C /Ro 84/.

III.5) CONCLUSIONS

In view of the results discussed above it seems reasonable to use graphite as a collector material for routine plasma measurements and to take silicon if special measurements as for example depth profiling of hydrogen are required. Papyex, though very often used in the past, seems not to be the appropriate material because of its large impurity concentration and low thermal resistivity. Rather pure graphite ($\sim$2 ppm) can be obtained from manufactors even in the desired forms and shapes.

Routine analysis of plasma exposed probes should be performed with RBS and PIXE alternatively.

If a low background of the impurities in question exists, PIXE spectra from collector probes may be easier in evaluation than RBS spectra. Additionally it can separate between stainless steel components, not possible with RBS. If depth discrimination is required, RBS has to be preferred, possibly with larger energies than 1 MeV. However, because of the effects mentioned, the value of depth profiling impurities on collector surfaces is doubtful.

IV) DESIGN AND CONSTRUCTION OF THE PROBE

A rough outline of the probe design was given in /Mö 83/ and an overview is shown in JET drawing SKL. 181/001 issue B, where the overall dimensions are defined.
The more detailed design described below was made in close collaboration with Culham laboratories (FTS), JET and Pfeiffer/Asslar (FRG) (SAS, PBPS). This was important as the probe has to fit to the manipulators of all three systems.

The probe design can be divided into three parts:
1) The probe interface where the probe is gripped by the manipulators of FTS, PBS and SAS.
2) The probe shield which surrounds the collector and protects it against heat loads.
3) The probe collector which has to be rotated during plasma exposure and where ions are collected.

The basic idea of the design was to obtain a module system of the three components mentioned above allowing to vary later on for example the collector without varying other components. This is important in view of the use of alternative collector materials mentioned in section III.5).

An overview of the existing probe design is given in Drawing 2B 1166-100. The following detail drawings show parts of the probe which can be identified in the master drawing by the last two underlined digits of the indicated numbers.

IV.1) Probe interface (Drawings: 3 D 1166 - 103b, - 104a,- 105, - 110 and 4 D 111b, - 112, - 113, - 114).

The interface consists of the outer and inner carrier (3 D 1166-104 a,- 103 b) the insulator (3D 1166-105) and components belonging to the rotatable axis (3D 1166-110 a, 4D 1166-111b, -112-113, - 114). The ball bearings are UHV-compatible. Rotation of the axis is enabled after withdrawing the pin(4D 1166-111b) which defines the datum position of the collector relative to the probe. Withdrawing is performed when the rotational part of the manipulator grips the axis. Thus rotation with negligible torque is possible. The holes in the collar of the outer and inner carrier are for a pin fixing the position of the probe in the trolley of the SAS. The grove in the inner carrier prevents rotation of the whole probe when it is gripped by the manipulator. The insulator allows the collector being biased relative to the plasma.

IV.2) Probe shield (Drawings: 3D 1166-102, - 107,- 109b)

The probe shield consists of a cylindrical shield a plate at the probe tip both made out of graphite and a support carrier. Graphite has proven to be a suitable material for the shield /Er 83/ as it has a high thermal resistivity, low Z and will not act as a source of heavy impurities as the stainless steel components are and which in turn will be investigated in JET.

The support carrier and the shield were constructed in such a way to prevent falling of the shield into the torus even when it brakes. The support carrier is screwed up with the outer carrier

of the interface. Hence the graphite cylinder is only clamped and set in a position defined by a pin and slot. Thus mechanical stresses are avoided. The thick graphite plate at the tip is crewed up with the support carrier by means of six screws. Slots in the graphite cylinder allow transmission of particles to the collector surface. The thickness of the slots and their width were performed such as to receive a good compromise between high transmission, good time resolution and stability. The corresponding slots in the underlaying support carrier must be considerably wider to avoid erosion of metal from the carrier by scattered particles and redeposition on the collector surface, which would lead to uncertainties in the determination of deposits from the plasma. This could also be avoided by using a material for the support carrier which can be clearly separated from plasma constituents. Also a suitable coating of the carrier would prevent uncertainties.

IV.3) Probe collector (drawings 3 D 1166-101,- 106, 4D 1166-108)

Similar to the probe shield the collector consists of a graphite cylinder of high purity which is clampled on a support carrier by means of a ring at the front side. The support carrier is connected with the axis of the probe by means of a screw and a defined datum position of the collector graphite cylinder is ensured by a pin and a grove in the cylinder.
In the SAS the collector will be analysed after exposure to the plasma without being dismounted from the probe and hence possible pollution of the surface can be avoided.

IV.4 MATERIALS

The materials proposed for the construction of the probe are indicated in the original drawing 2B 1166-100.
Thereafter the following parts should be made out of:
Inconel 600: Support carrier for the shield (BD 1166-102)
outer carrier for the probe interface
(3 D 1166 - 103b)

inner carrier for the probe interace
(3 D 1166 - 104a)

Cu Al 10 Fe: pin a part (4 D 1166 - 111)
part (4 D 1166 - 111)

Graphite: plate (3 D 1166 - 109)
shield (3 D 1166 - 107)
collector (3 D 1166 - 106)
for the plate and shield and collector the graphite should be very pure (ppm) and for the collector the outer surface roughness should be below 2 um.

Al_2O_3: insulating part (3 D - 1166 - 105)

The bearings must be UHV compatible. All other parts can be made out of stainless steel. The contact spring (4 D 1166 - 112) must be able to withstand 500^0 C.

Acknowledgement

We would like to thank Mr. H. Kukral for preparing the metal films on the samples and performing the SEM and EIXE measurements as well as Mr. H. Schmidl and Mr. A. Wiederer for the technical assistence with the accelerator measurements.

V) REFERENCES

/Bø 84/ P. Børgesen, L. Svendsen and J. Ehrenberg to be published.

/St 78/ P. Staib and G. Staudenmaier, J. Nucl. Mat. 76 & 77 (1978), 78

/McCr 79/ G. M. McCracken and P.E. Stott, Nucl. Fusion 19/7 (1979) 889

/Ta 82/ E. Taglauer, B.M. U. Scherzer, P. Varga, R. Behrisch, Chen-Cheng Kai and the ASDEX-Team, J. Nucl. Mat. 111 & 112 (1982) 1323

/Wi 82/ J. P. Withrow, R.A. Zuhr and J. Roth, J. Vac. Sci. Technol. 20 (1982) 1323

/Ho 82/ Y. Hori, A. Sagara, Z. Kabeya, J. Onodera, K. Akaishi, K. Kamada, A. Miyahara, S. Mamiya, S. Tanshi and J. Fujita, J. Nucl. Mat. 111 & 112 (1982) 137

/Ch 78/ W.-K. Chu, J.W. Mayer and M.A. Nicolet, "Backscattering Spectrometry", Academic Press, N.Y. 1978

/Jo 76/ S.A.E. Johansson and T.B. Johansson, Nucl. Instr. Meth. 137 (1976) 473

/St 77/ P. Staib and G. Staudenmaier, Proc. Int. Vac. Congress and 3rd Int. Conf. on Solid Surfaces (1977), Vienna, p. 2355

/Gl 80/ E. Glock and Pulsator-Team, J. Nucl. Mat. 93 & 94 (1980) 305

/Be 84/ R. Behrisch, P. Børgesen, J. Ehrenberg, A.P. Martinelli, B.M.U. Scherzer, to be published

/Ro 84/ J. Roth, private communication

/Er 83/ K. Ertl, private communication

/Mö 83/ W. Möller, IPP-JET Report No 11, Jan. 1983

VI) FIGURE CAPTIONS

Fig.1 Rutherford backscattering (RBS) spectra of various graphite samples at a) 300 K and after heating to b) 840 K and c) 930 K.

Fig.2 Protons induced X-ray emission (PIXE) spectra of various graphite samples at a) 300 K, and b) after heating to 930 K.

Fig.3 RBS spectra of a 100 A Ni layer on a) vitreous graphite and b) silicon at 300 K and after heating to 1090 K.

Fig.4 Ni droplet formation on various graphite and silicon surfaces after heating to 1090 K.

Fig.5 Electron induced X-ray emission (EIXE) spectra on vitreous graphite: a) electron beam focused onto a droplet, b) electron beam focused in between droplets.

Fig.6 Electron induced X-ray emission (EIXE) spectra on silicon: a) electron beam focused onto a droplet, b) electron beam focused in between droplets.

Fig.7 Analysis of a time resolved collector measurement in a plasma discharge a) with RBS and b) with PIXE. Pd was evaporated onto the collector surface. c) Variation of plasma parameters during discharge.

J_p = Plasma current t = time resolution of exposure
n = plasma density
NI = Neutral Injection

Fig.8 Analysis of stationary collector measurement of a plasma discharge, a) with RBS, b) with PIXE. -d- gives the position of the aperture in front of the collector surface.

Fig.9 Comparison of surface topographies of Papyex before and after heat loads in plasma discharges.

VII) List of Tables

Table 1 Impurity concentrations in various graphite samples measured by RBS and PIXE after heating to various temperatures.

Table 2 Variation of Ni films and impurities on various samples after heating to various temperatures measured by RBS and PIXE

VIII) Captions of Probe and component drawings

Drawing		
Drawing	2B 1166 - 100	probe overview
	3D 1166 - 101	support carrier for the collector
	- 102	support carrier for the shield
	- 103 b	outer carrier for the probe interface
	- 104 a	inner carrier for the probe interface
	- 105	insulating part
	- 106	collector
	- 107	probe shield
	- 108	ring for the collector
	- 109 b	front plate for the shield
	- 110 a	probe axis
	4D 1166 - 111 b	pin
	" - 112	contact spring
	- 113	sleeve
	- 114	pin

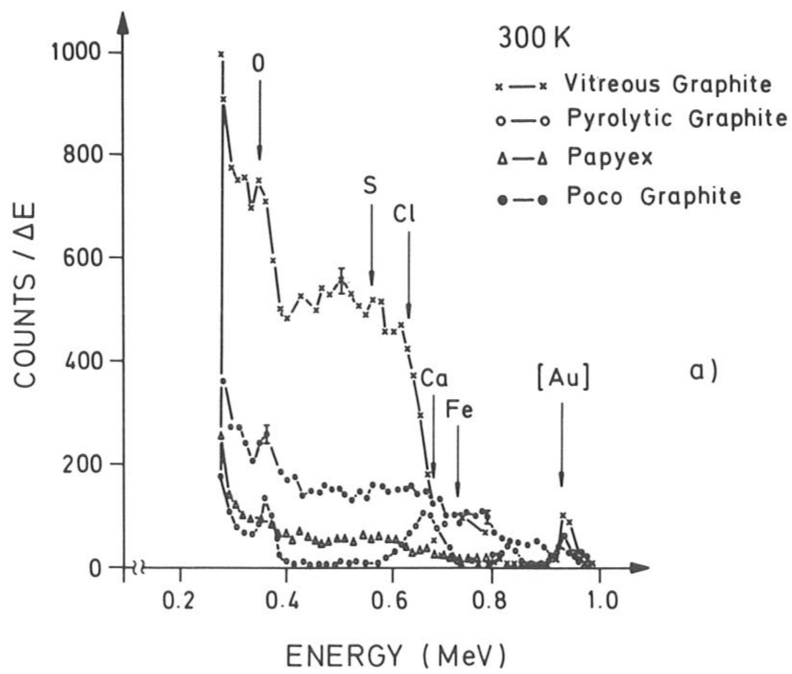

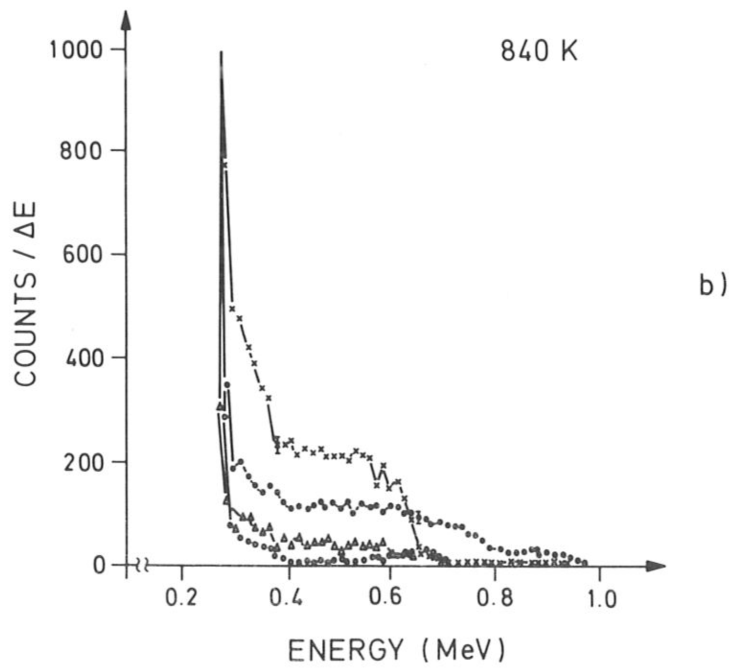

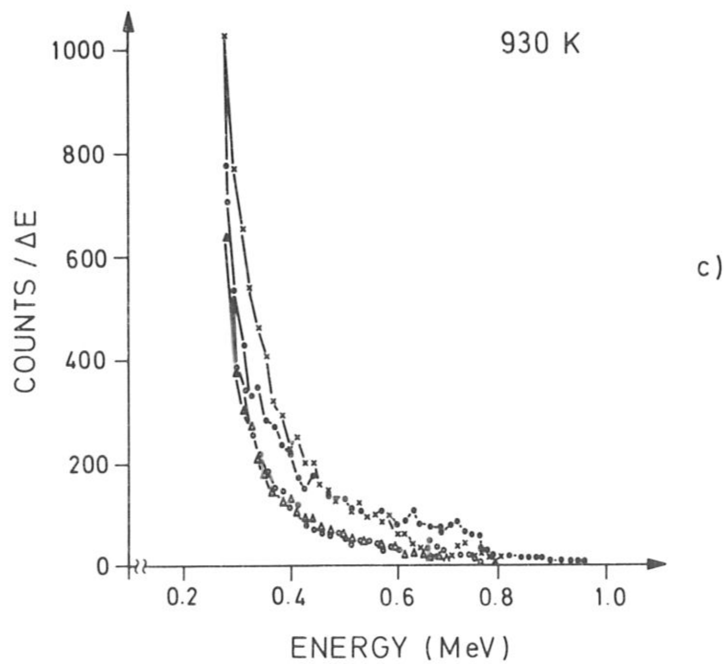

g. 1

$S_{k\alpha}$

$Cl_{k\alpha}$

300 K

Vitr. Graphite

Pyr. Graphite

Papyex

Poco Graphite

a)

V(kα)

Ca(kα)

Fe(kα)

COUNTS / ΔE

ENERGY (keV)

930 K

b)

COUNTS / ΔE

ENERGY (keV)

Fig. 2

a)

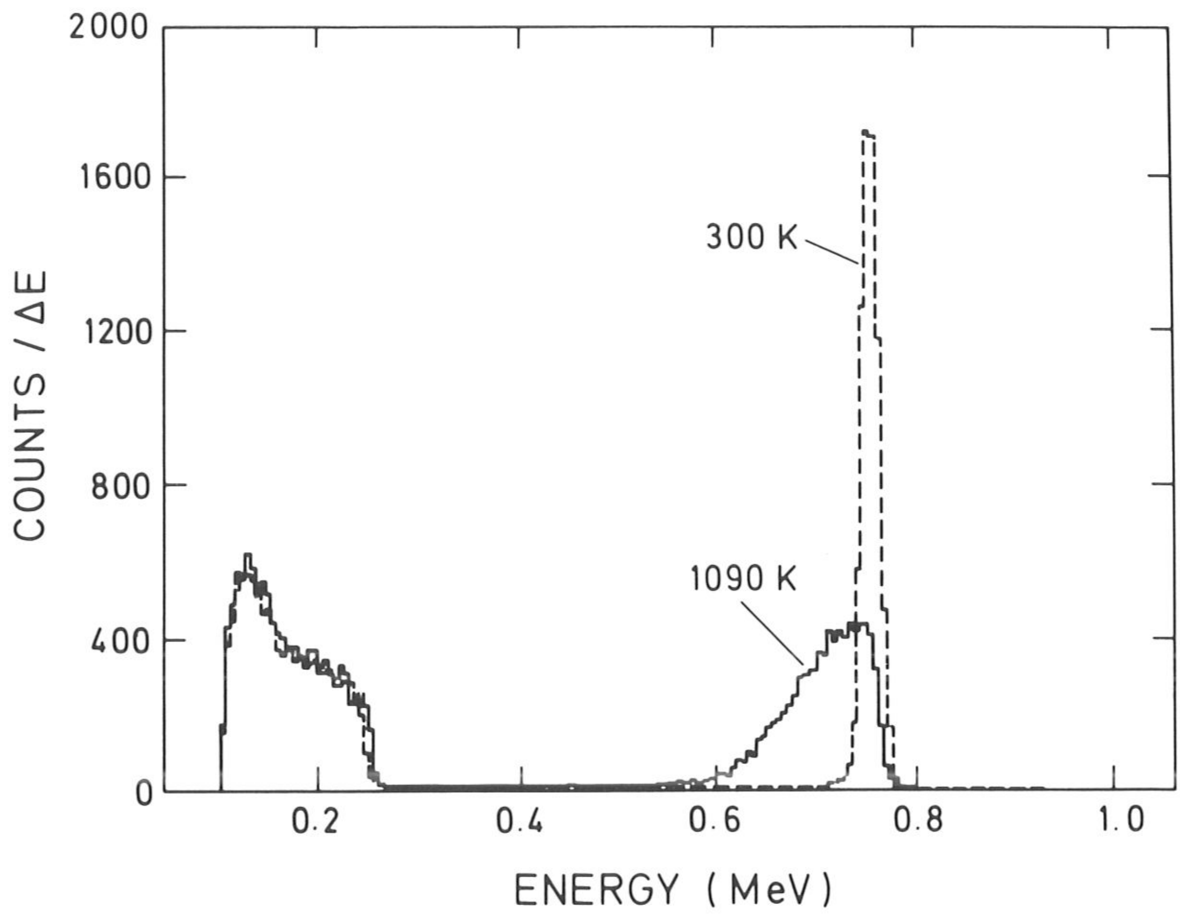

b)

2000
1600
1200
800
400
0
COUNTS / ΔE
1090 K
300 K
0.2
0.4
0.6
0.8
1.0
ENERGY (MeV)

· 3

100 Å Ni on graphite and silicon surfaces

T = 1090 K

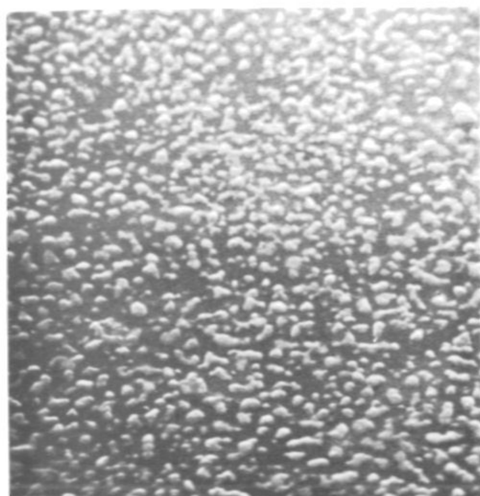

Vitreous graphite

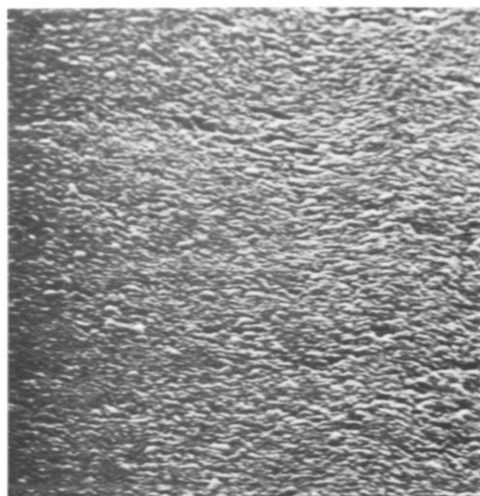

Pyrolytic graphite

Papyex

2 μm

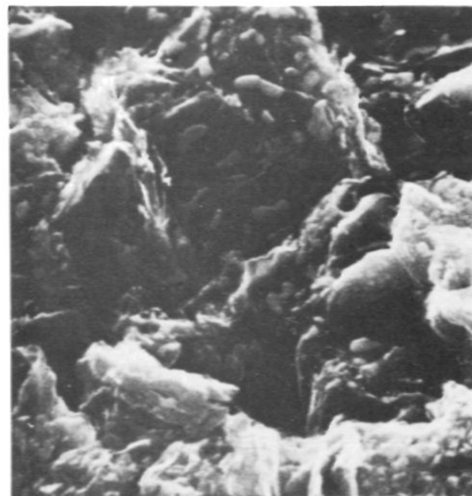

Poco graphite

Silicon (111)

Fig. 4

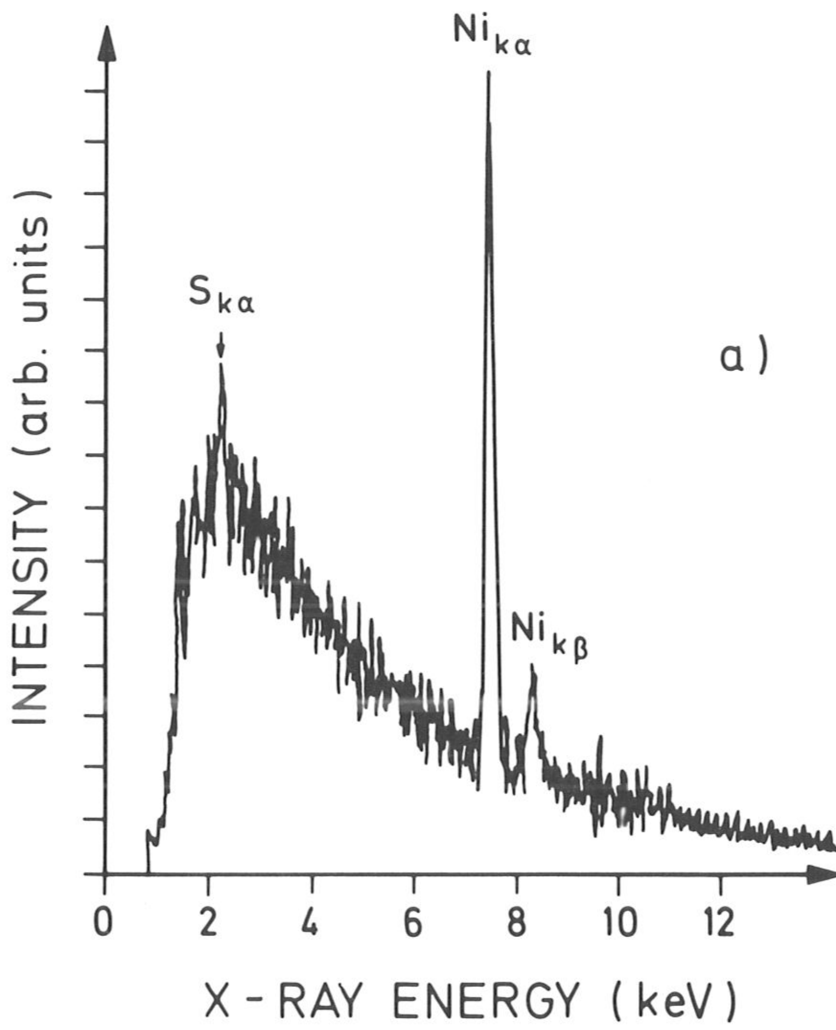

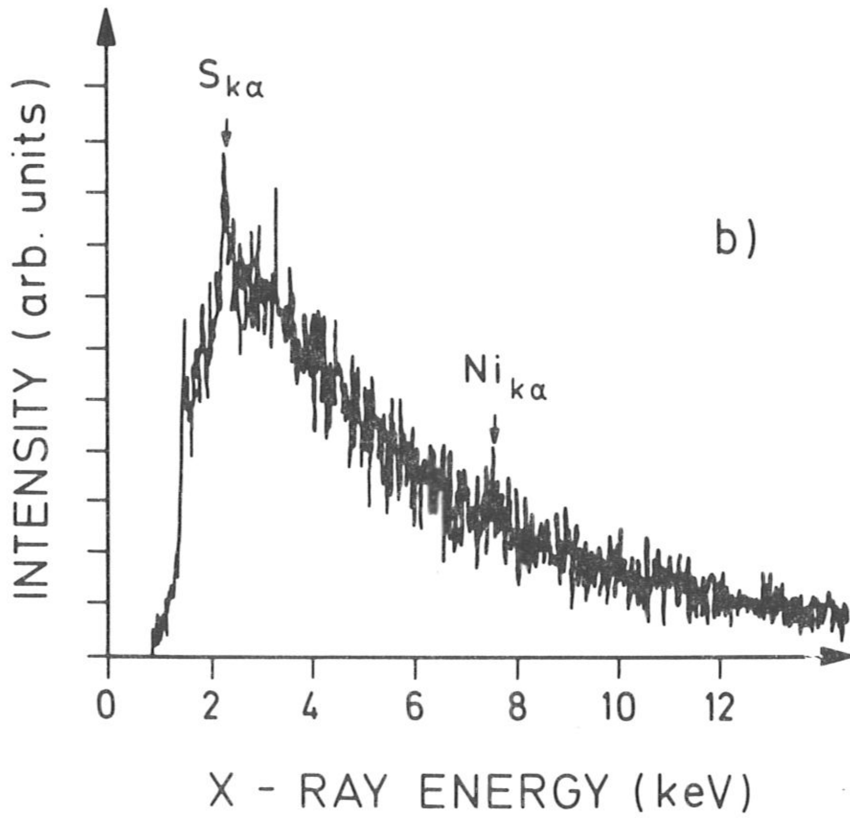

ig. 5

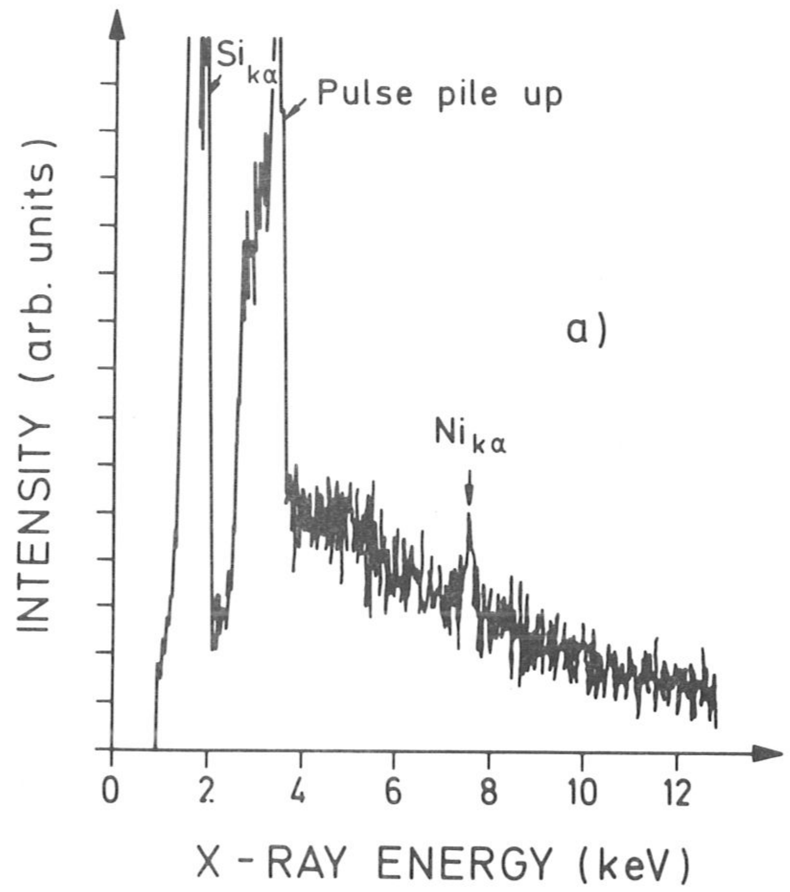

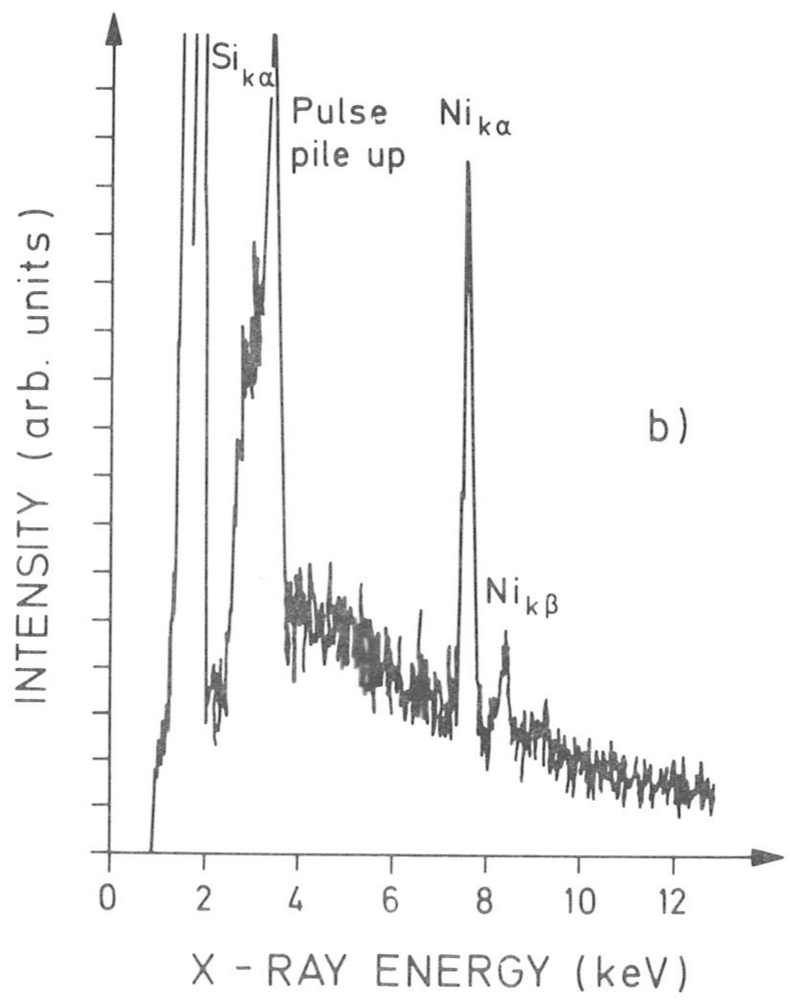

Fig. 6

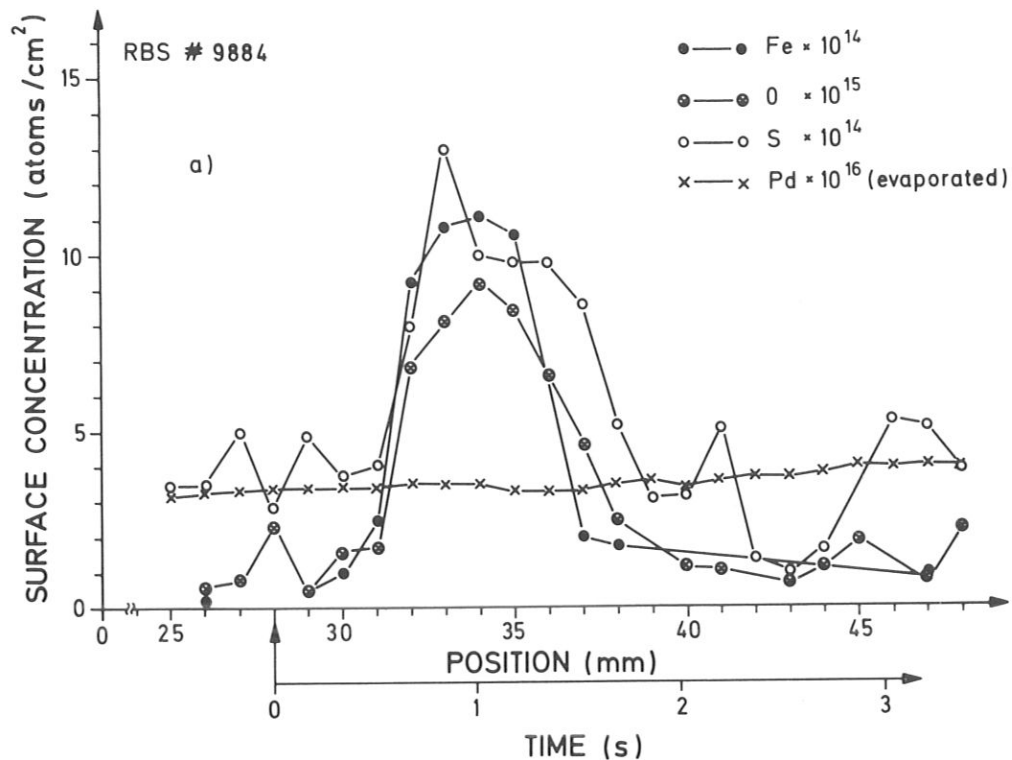

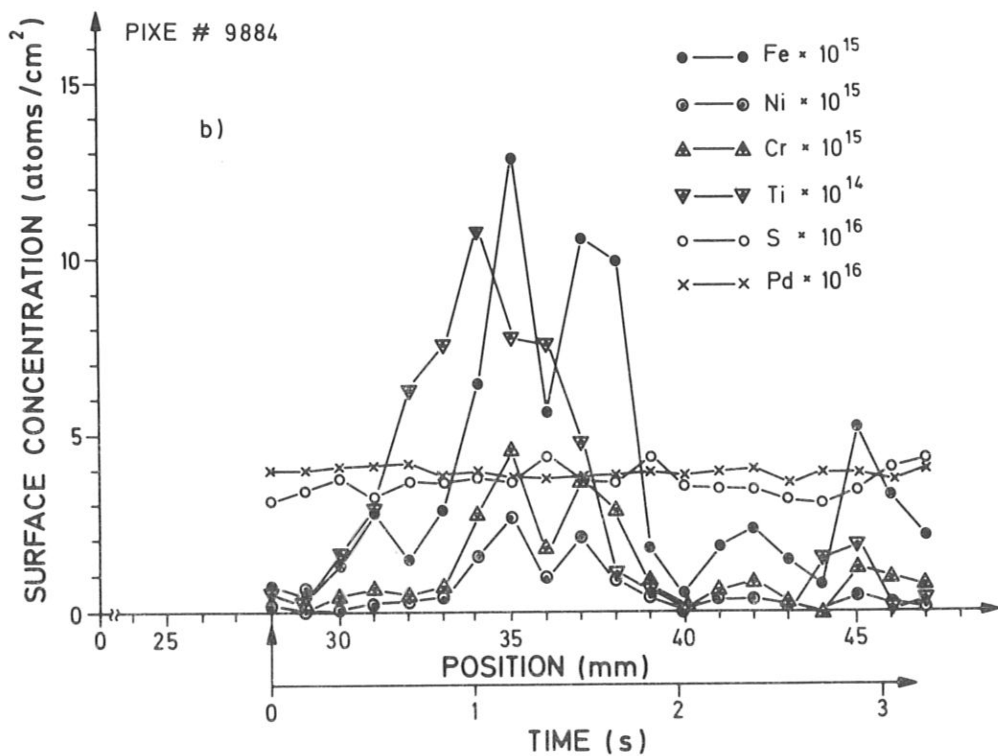

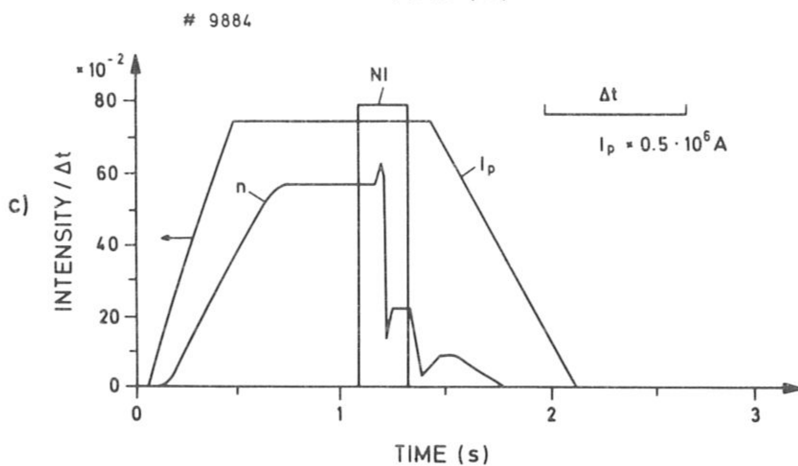

Fig. 7

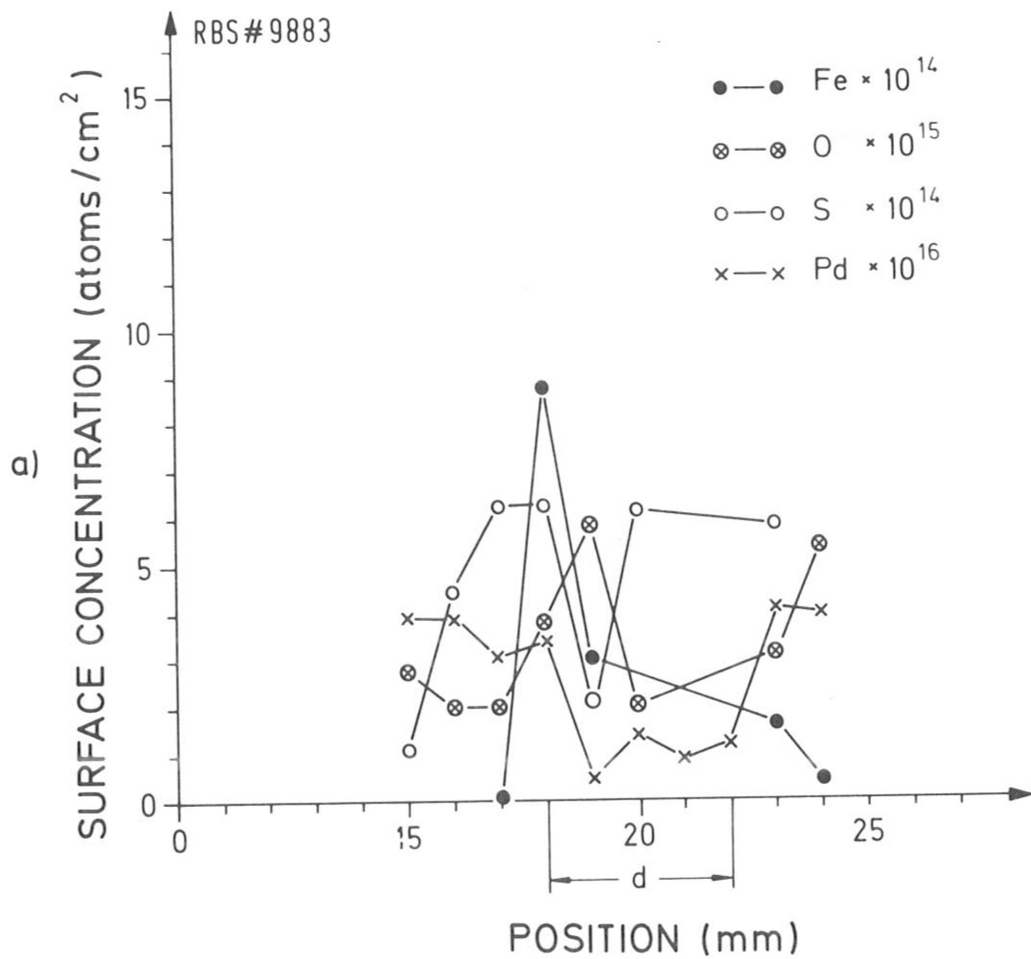

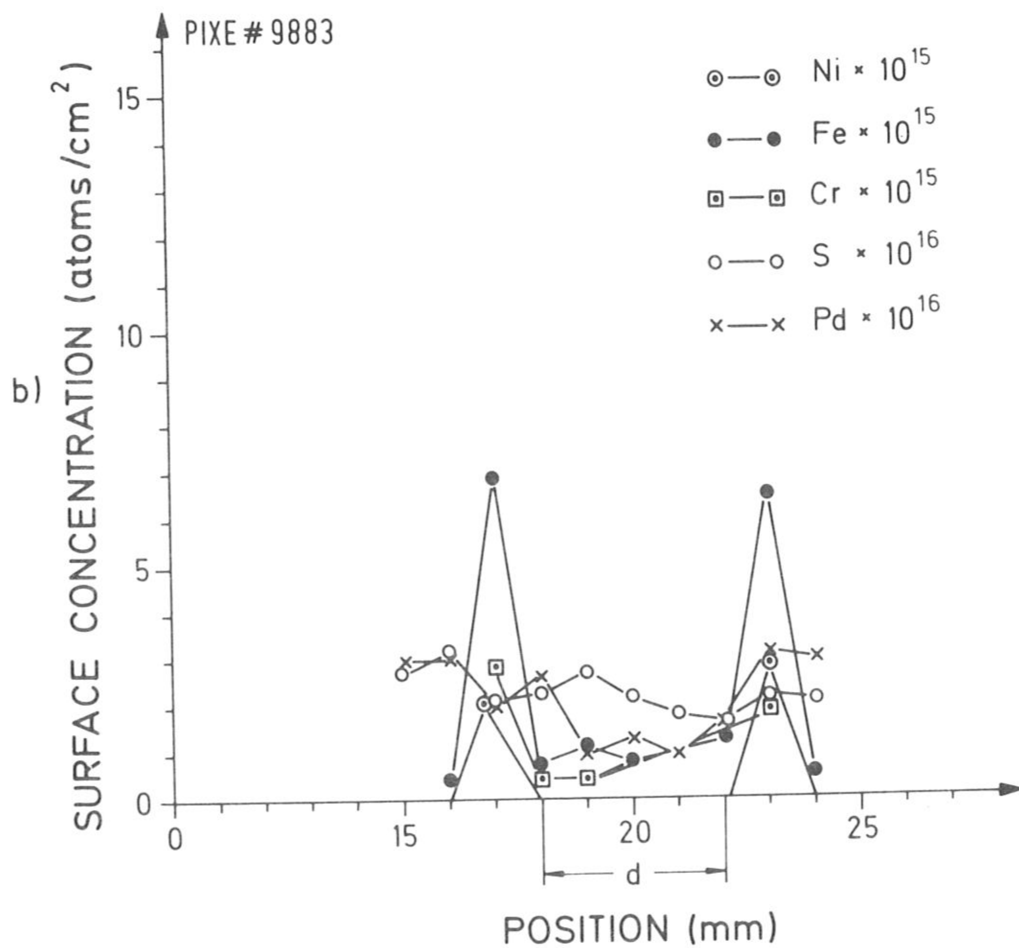

Fig. 8

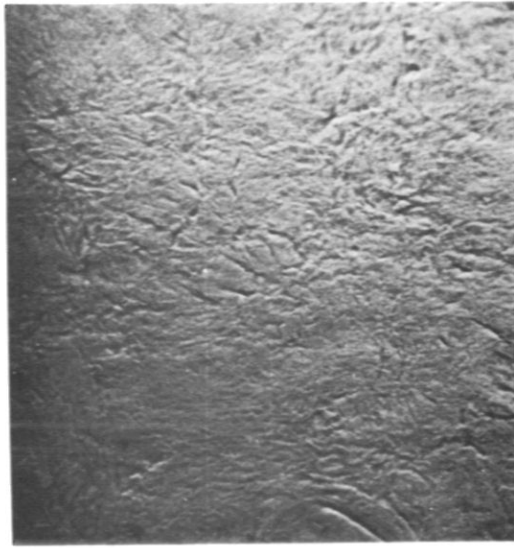

Papyex
as received

0.2 mm

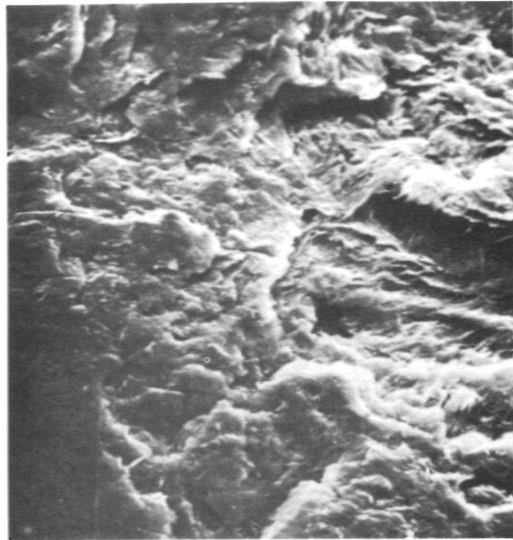

Papyex
after heatload

Fig. 9

Table 1

		RBS								PIXE					
		O	S	Cl	K	Ca	V	Fe	Cs	S	Cl	K	Ca	V	Fe
300 K	Vitr. Graphite	$4x10^{15}$	$9x10^{-4}$	x	x	-	-	$4x10^{-5}$	$1x10^{14}$	$2.3x10^{16}$ $2.5x10^{-4}$	$1.5x10^{16}$ $1.5x10^{-4}$	$5.7x10^{14}$ $5.4x10^{-6}$	-	-	-
	Pyr. Graphite	$3x10^{15}$	$2x10^{14}$	x	x	x	-	-	$7x10^{13}$	$< 10^{15}$ $< 10^{-5}$	$<10^{14}$ $<10^{-6}$	-	$< 10^{15}$ $< 10^{-5}$	-	-
	Poco Graphite	$4x10^{15}$	x	x	x	x	$8x10^{-4}$	x	x	-	-	-	$3x10^{15}$ $3x10^{-5}$	$2.8x10^{16}$ $2.6x10^{-4}$	$5x10^{15}$ $5x10^{-5}$
	Papyex	$1x10^{15}$	$3x10^{-4}$	$2x10^{-4}$		$9x10^{-6}$		$5x10^{-5}$	x	$2.9x10^{16}$ $3 x10^{-4}$	$1.5x10^{15}$ $1.5x10^{-5}$	-	$2.7x10^{15}$ $2.7x10^{-5}$	-	$1x10^{15}$ $1x10^{-5}$
	Silicon	-	-	-	-	-	-	-	-	-	-	-	-	-	-
840K	Vitr. Graphite	$2x10^{15}$	$1x10^{-3}$	x	$2x10^{-4}$	-	-	$4x10^{-5}$	-						
	Pyr. Graphite	$2x10^{14}$	<	x	x	$2x10^{-4}$	-	-	-						
	Poco Graphite	$8x10^{14}$	x	x	x	x	$2x10^{-4}$	$1x10^{-4}$	-						
	Papyex	<	<	<	x	<	-	$5x10^{-5}$	-						
	Silicon	-	-	-	-	-	-	-	-						
930 K	Vitr. Graphite	<	<	x	<	-	-	x	-	$4.4x10^{16}$ $4.4x10^{-4}$	$<10^{14}$ $<10^{-6}$	$5.7x10^{14}$ $5.4x10^{-6}$	-	-	-
	Pyr. Graphite	<	<	x	x	$2x10^{-4}$	-	$2x10^{-4}$	-	$< 10^{15}$ $< 10^{-5}$	$<10^{14}$ $<10^{-6}$	-	$< 10^{15}$ $< 10^{-5}$	-	-
	Poco Graphite	<	$6x10^{-4}$	x	x	$1x10^{-4}$	$4x10^{-4}$	x	-	-	-	-	$6x10^{14}$ $6x10^{-6}$	$1x10^{16}$ $1x10^{-4}$	$5x10^{14}$ $5x10^{-6}$
	Papyex	<	$5x10^{-4}$	$4x10^{-4}$	x	x	-	$1x10^{-4}$	-	$2x10^{16}$ $2x10^{-4}$	$<10^{14}$ $<10^{-6}$	-	$1x10^{15}$ $1x10^{-5}$	-	$2x10^{14}$ $2x10^{-6}$
	Silicon	-	-	-	-	-	-	-	-	-	-	-	-	-	-

x Peak possible but not evaluated due to high background $(< 1 \cdot 10^{14}$ ats/cm$^2)$ $(< 1 \cdot 10^{-6}$ ats/c-atom)

< Peak detected and reduced relative to foregoing temperature, but not evaluated due to high background

\- No peak detected

Quantities with positive exponents in atoms/cm^2.
Quantities with negative exponents in atoms/carbon atom.

Table 2

		RBS			PIXE					
		Ni	width Å	O	Ni	S	K	Ca	V	Fe
300 K	Vitreous Graphite	1.1×10^{17}	150	1×10^{17}	0.9×10^{17}	7×10^{16} 7×10^{-4}	4×10^{15} 4×10^{-5}	1×10^{15} 1×10^{-5}	-	2×10^{15} 2×10^{-5}
	Pyr. Graphite	1.2×10^{17}	137	4.7×10^{16}	1.1×10^{17}	2×10^{15} 2×10^{-5}	$< 10^{15}$ $< 10^{-5}$	$< 10^{15}$ $< 10^{-5}$	-	-
	Poco Graphite	1.1×10^{17}	175	6×10^{16}	1.1×10^{17}	$< 10^{15}$ $< 10^{-5}$	$< 10^{15}$ $< 10^{-5}$	4×10^{15} 4×10^{-5}	4×10^{15} 4×10^{-5}	3×10^{15} 3×10^{-5}
	Papyex	1.2×10^{17}	136	3.4×10^{16}	1.1×10^{17}	2×10^{16} 2×10^{-4}	$< 10^{15}$ $< 10^{-5}$	2×10^{15} 2×10^{-5}	-	4×10^{15} 4×10^{-5}
	Silicon	1.3×10^{17}	133	-	1.0×10^{17}	-	-	-	-	-
620 K	Vitreous Graphite	1.1×10^{17}	132	6.1×10^{16}						
	Pyr. Graphite	1.1×10^{17}	136	1.8×10^{16}						
	Poco Graphite	1.1×10^{17}	139	2.8×10^{16}						
	Papyex	1.2×10^{17}	128	2.5×10^{16}						
	Silicon	1.2×10^{17}	129	-						
830 K	Vitreous Graphite	1.2×10^{17}	132	3.8×10^{16}						
	Pyr. Graphite	1.2×10^{17}	143	1.6×10^{16}						
	Poco Graphite	1.1×10^{17}	142	2.8×10^{16}						
	Papyex	1.2×10^{17}	132	1.6×10^{16}						
	Silicon	1.3×10^{17}	130	-						
1090 K	Vitreous Graphite	1.1×10^{17}	736	3.4×10^{16}	1.2×10^{17}	1×10^{17} 1×10^{-3}	6×10^{15} 6×10^{-5}	2×10^{15} 2×10^{-5}	-	4×10^{15} 4×10^{-5}
	Pyr. Graphite	1.0×10^{17}	380	2.2×10^{16}	1.1×10^{17}	2×10^{15} 2×10^{-5}	$< 10^{15}$ $< 10^{-5}$	$< 10^{15}$ $< 10^{-5}$	-	$< 10^{15}$ $< 10^{-5}$
	Poco Graphite	1.0×10^{17}	610	5.7×10^{16}	1.3×10^{17}	$< 10^{15}$ $< 10^{-5}$	$< 10^{15}$ $< 10^{-5}$	5×10^{15} 5×10^{-5}	5×10^{15} 5×10^{-5}	5×10^{15} 5×10^{-5}
	Papyex	1.1×10^{17}	1120	3.8×10^{16}	1.2×10^{17}	2×10^{16} 2×10^{-4}	$< 10^{15}$ $< 10^{-5}$	2×10^{15} 2×10^{-5}	-	6×10^{15} 6×10^{-5}
	Silicon	1.1×10^{17}	1500	-	0.9×10^{17}	-	-	-	-	-

- impurity not detected.

Quantities with positive exponents in atoms/cm^2

Quantities with negative exponents in atoms/carbon atom.

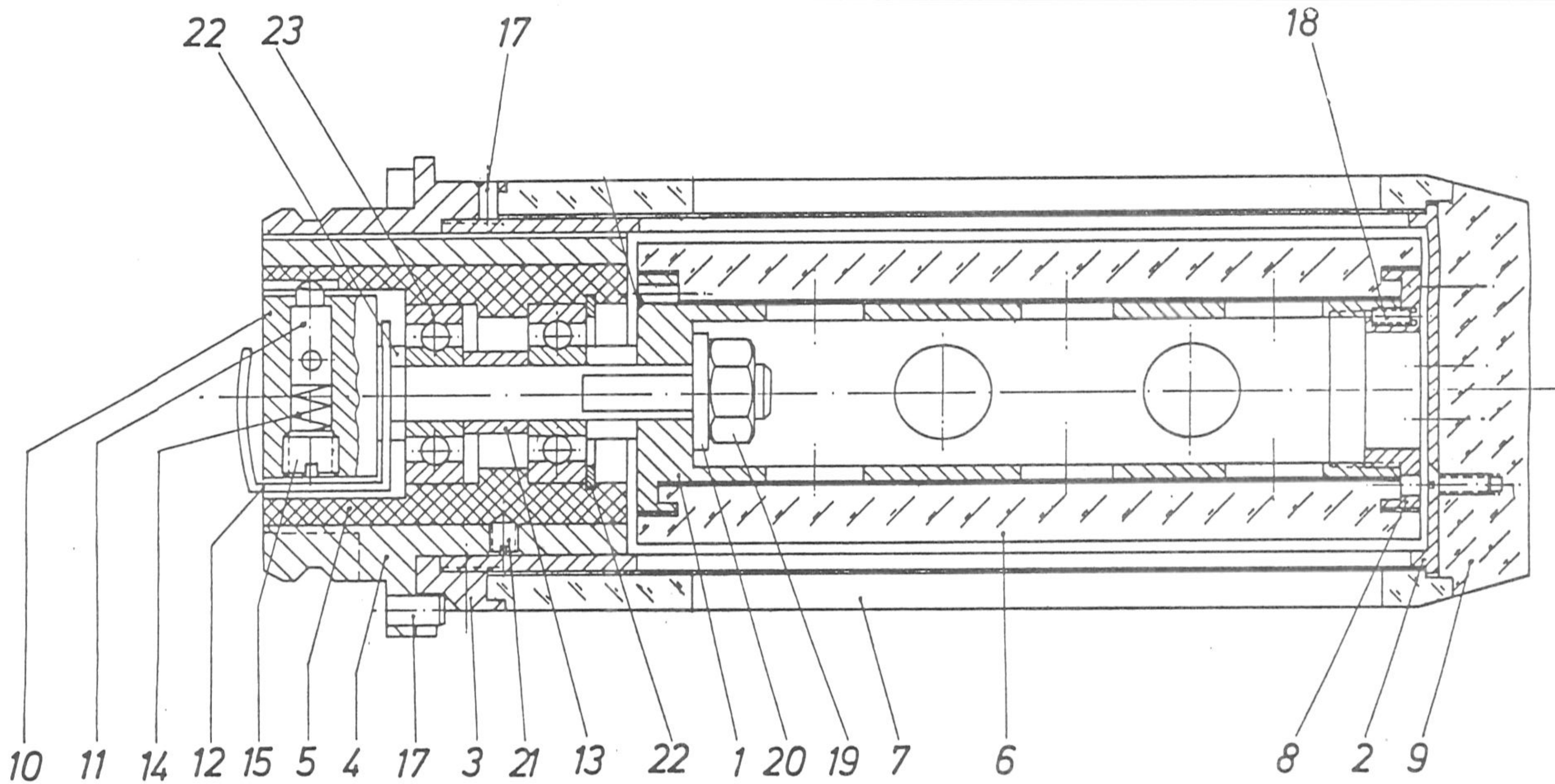

2 B 1166 – 100

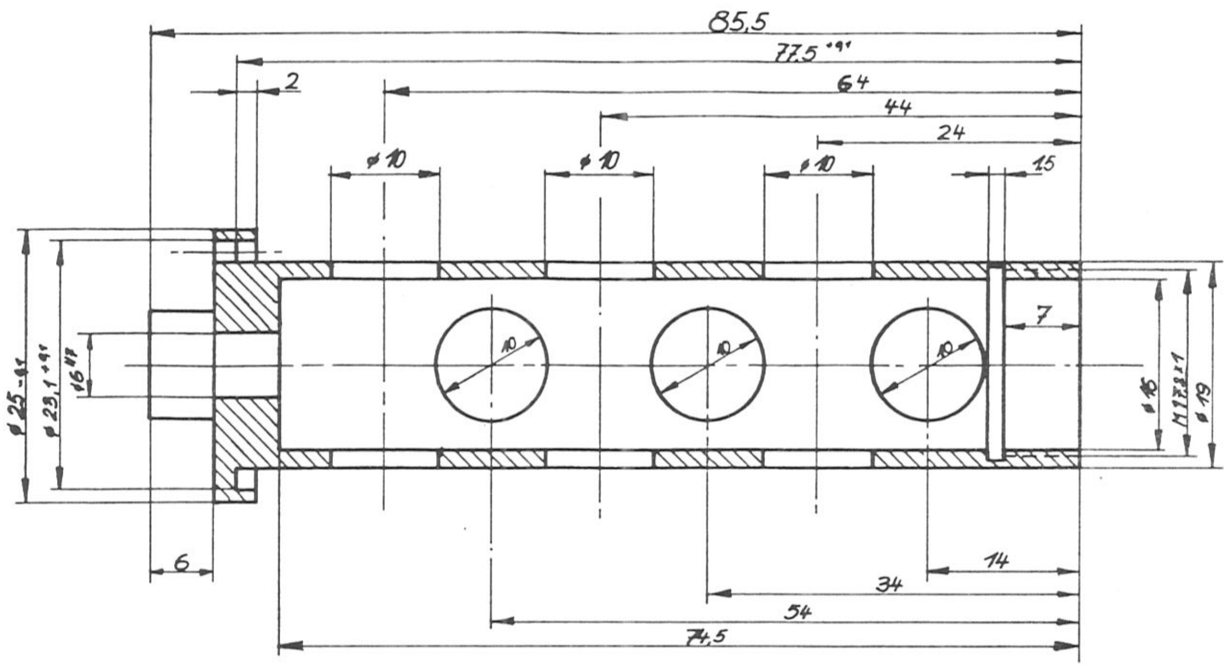
85,5
77,5 +0,1
2
64
44
24
⌀ 10
⌀ 10
⌀ 10
1,5
⌀ 25 -0,1
⌀ 23,1 +0,1
⌀ 6 H7
10
10
10
7
⌀ 16
M 17,8 x 1
⌀ 19
6
14
34
54
74,5

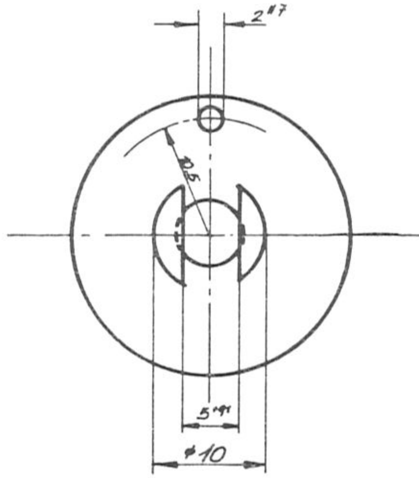
2 H7
10,5
5 +0,1
⌀ 10

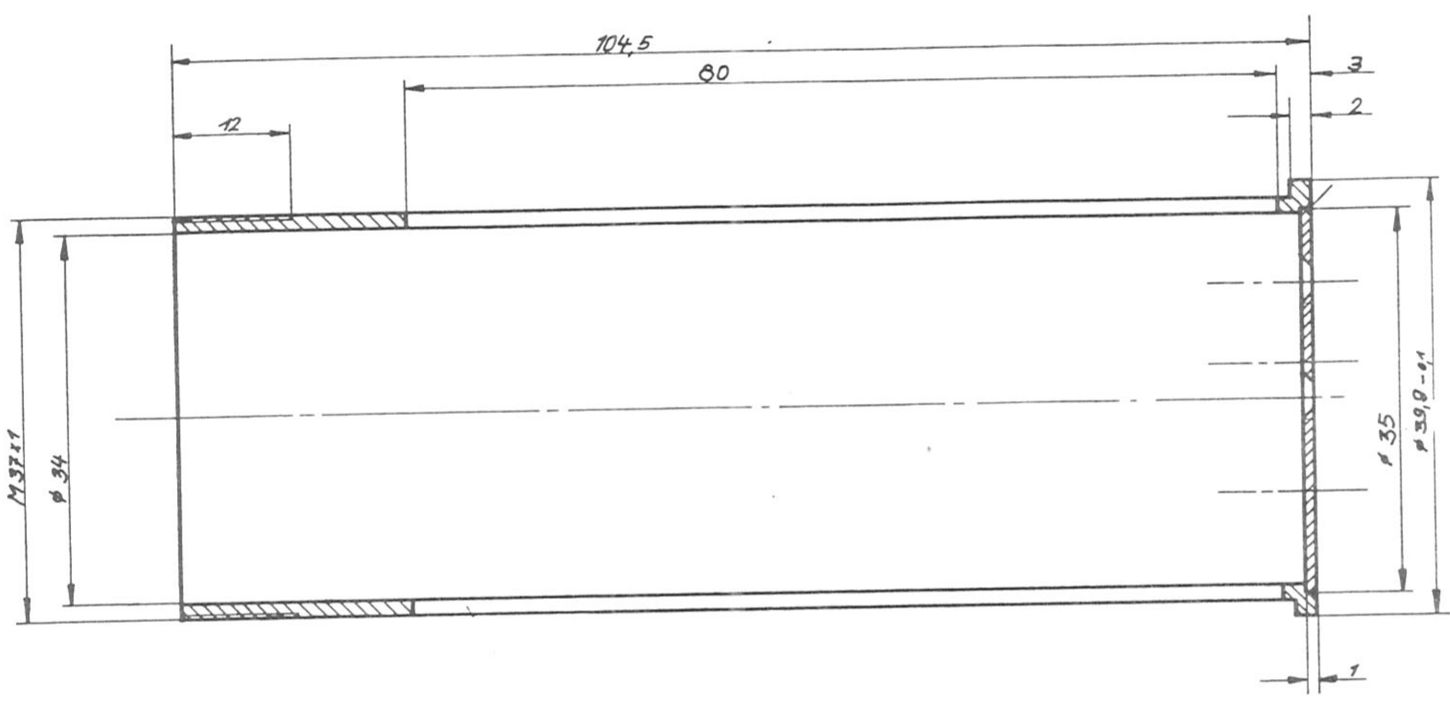

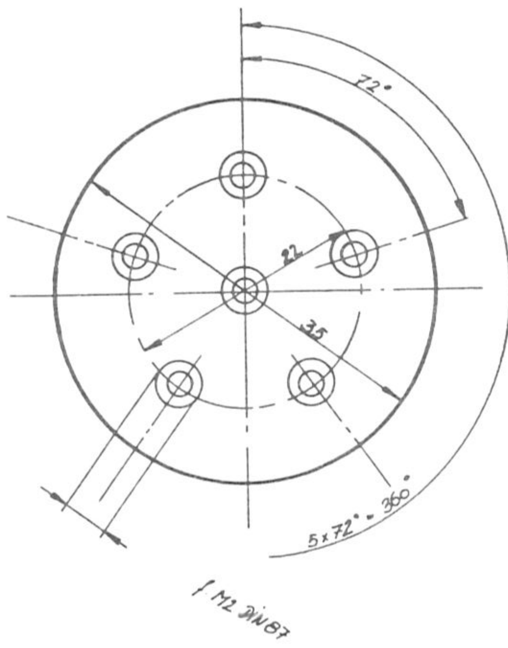

3D 1166 - 102

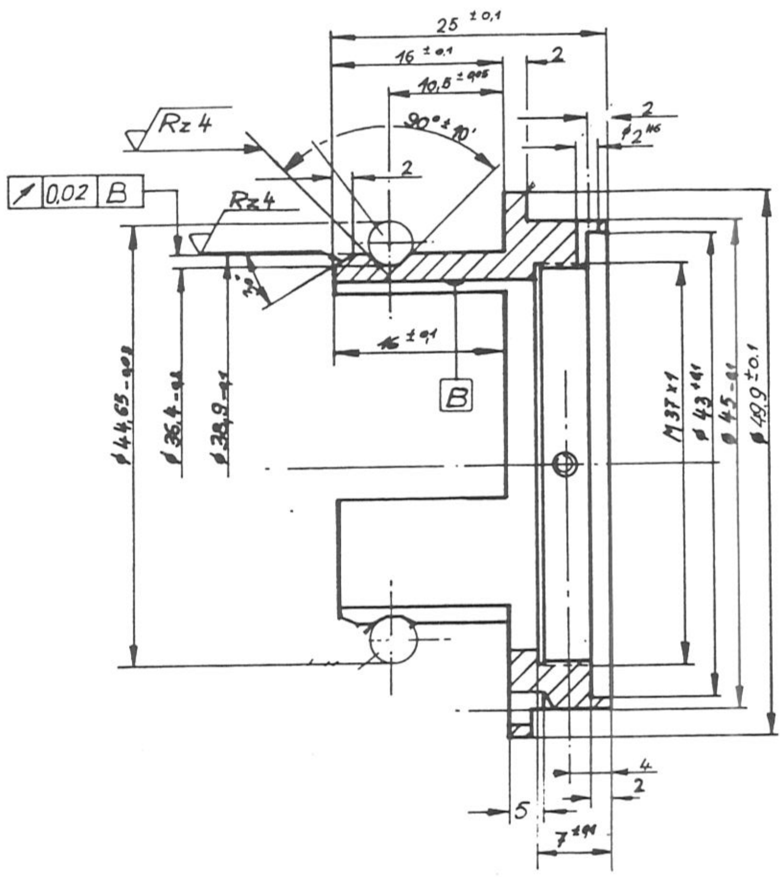

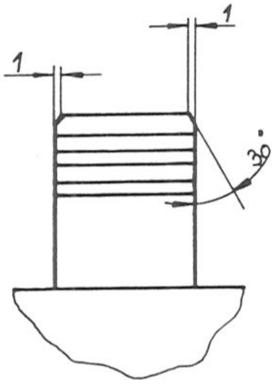

A

A

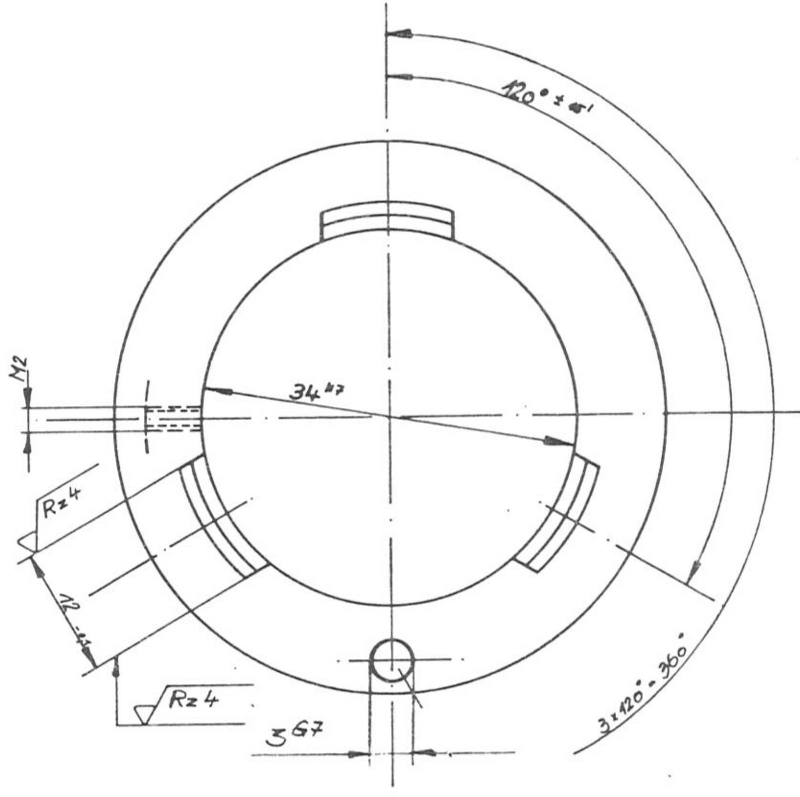

3D 1166 - 103b

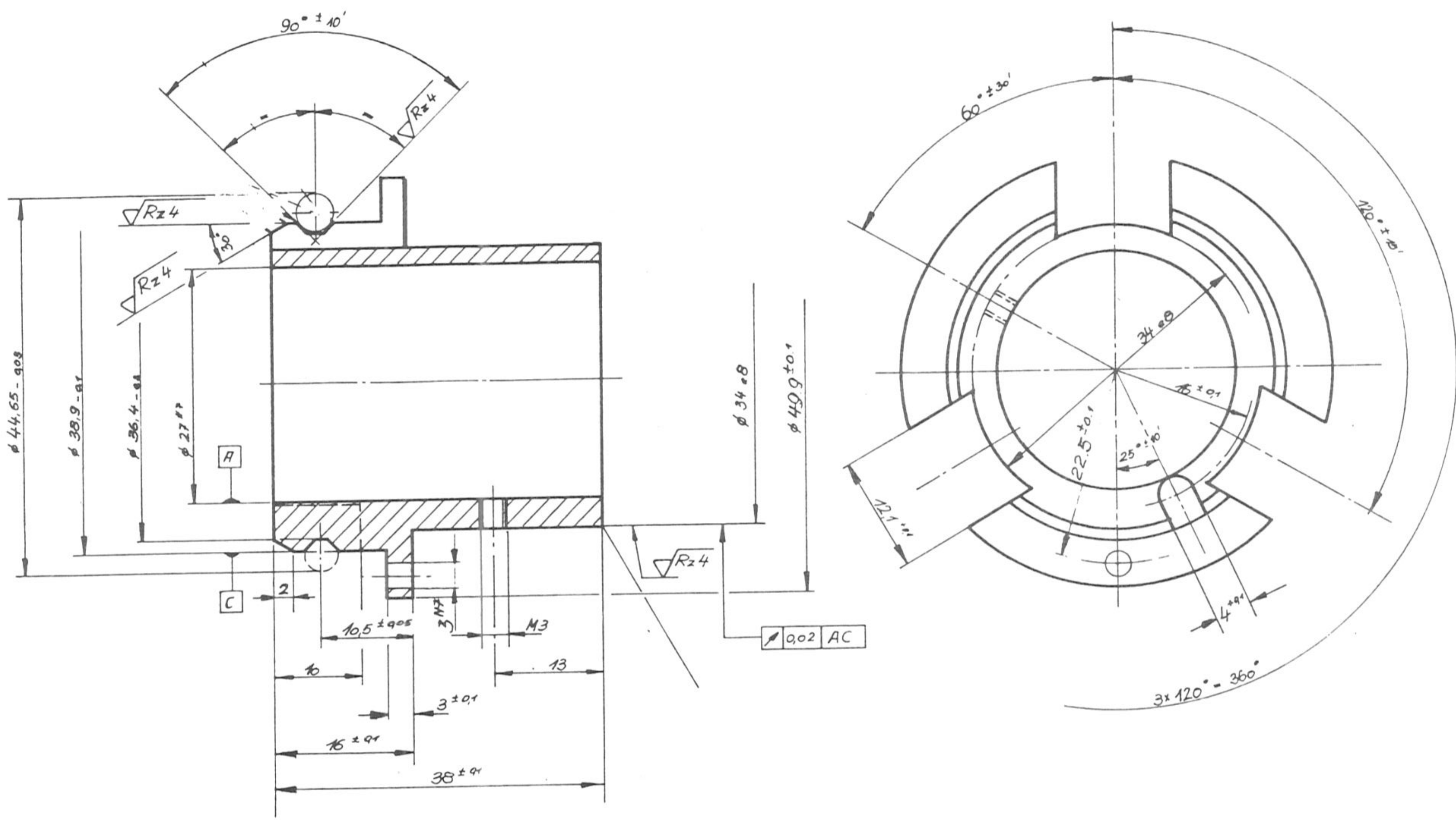

3 D 1166 - 104a

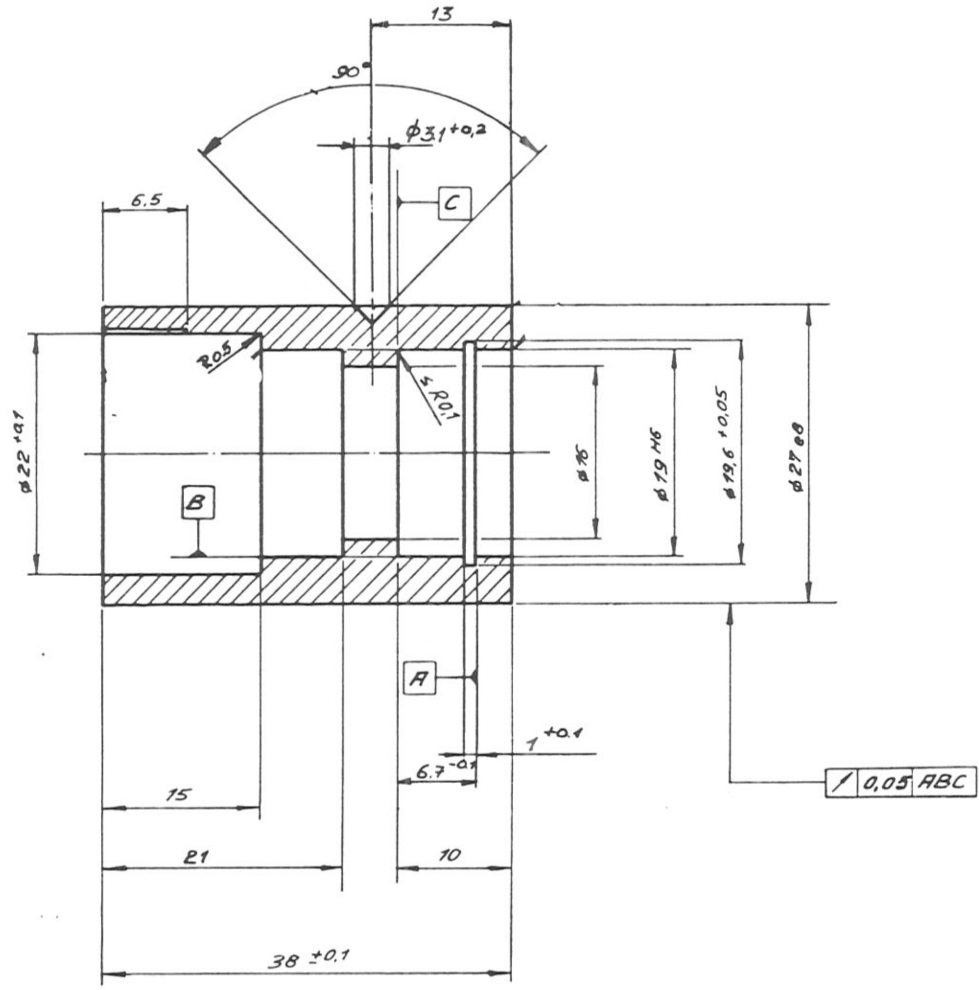

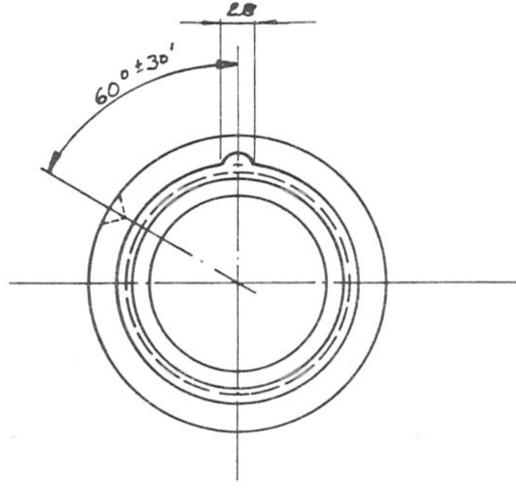

3D 1166 - 105

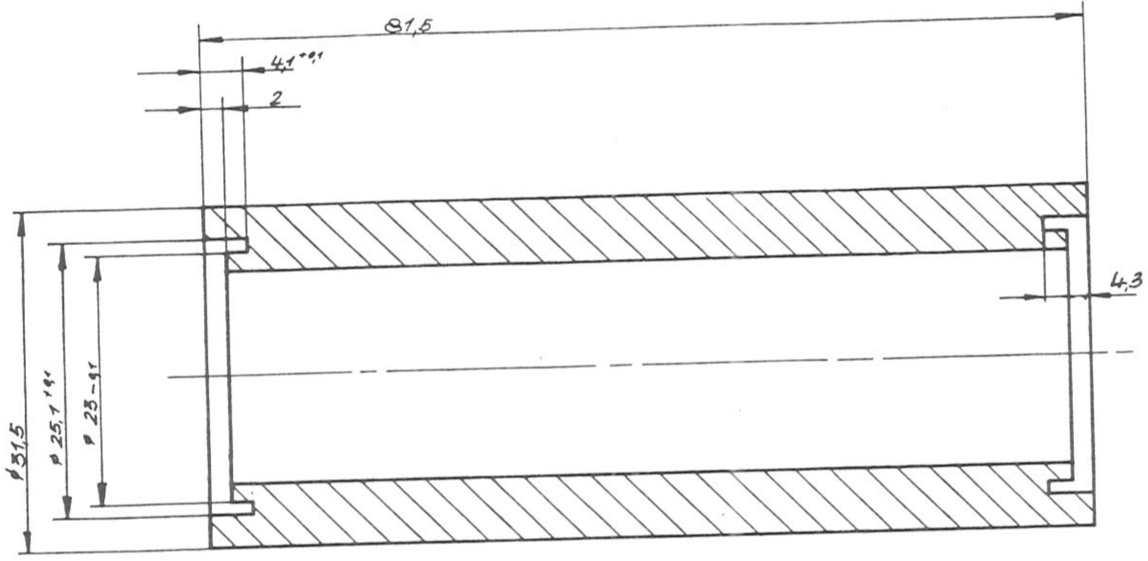

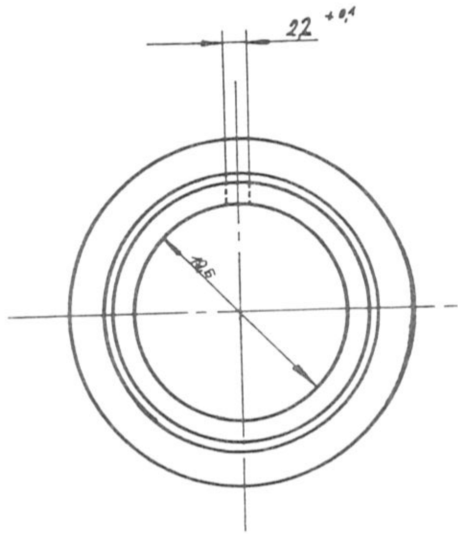

3D 1166 - 106

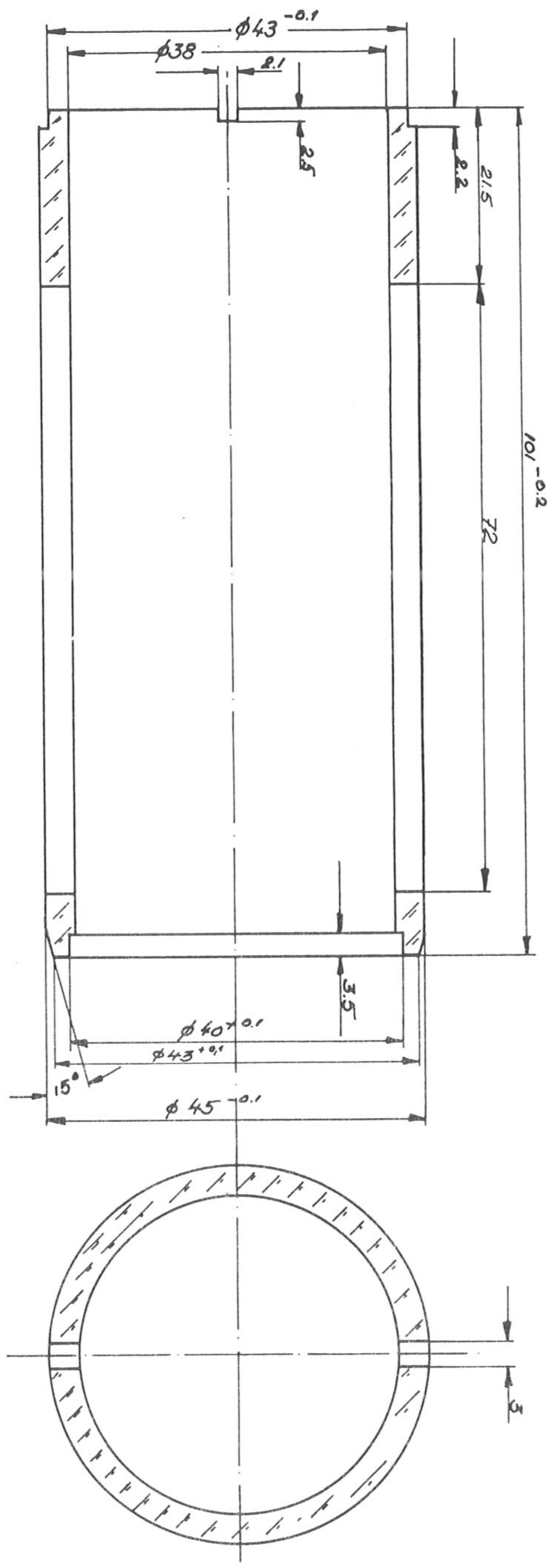

3D 1166-107

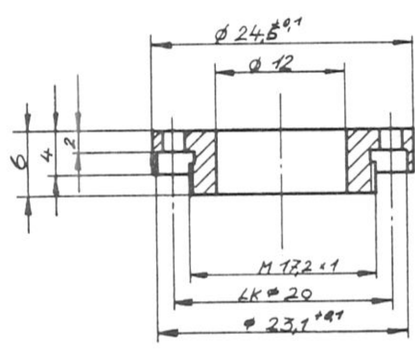

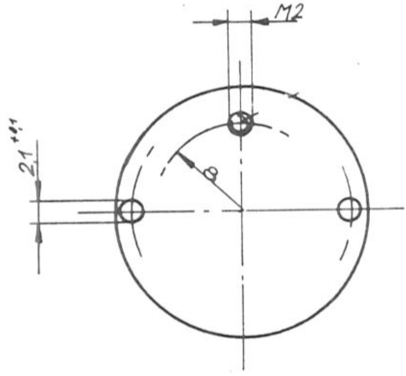

4D 1166 - 108

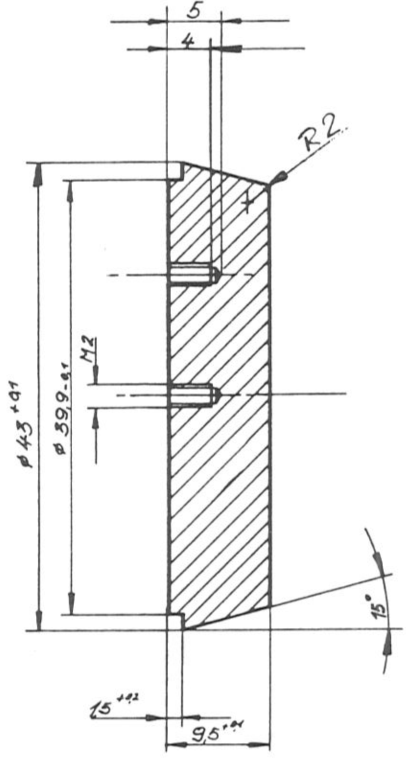

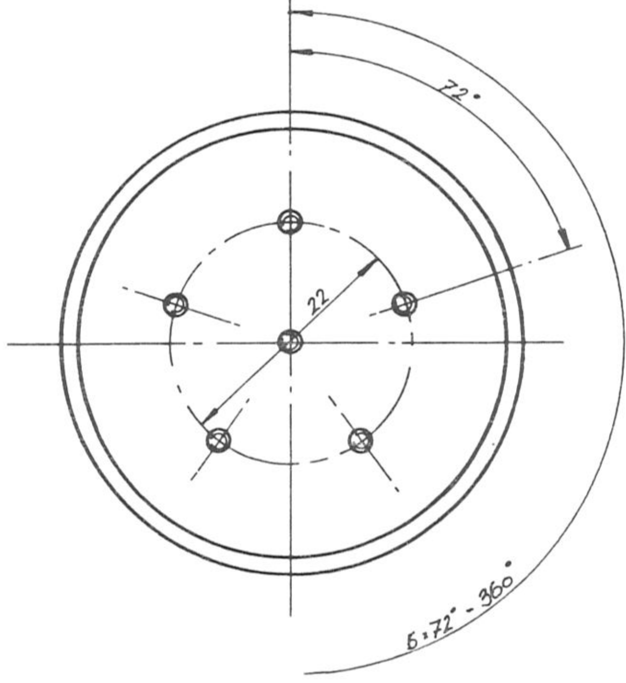

3D 1166 - 109b

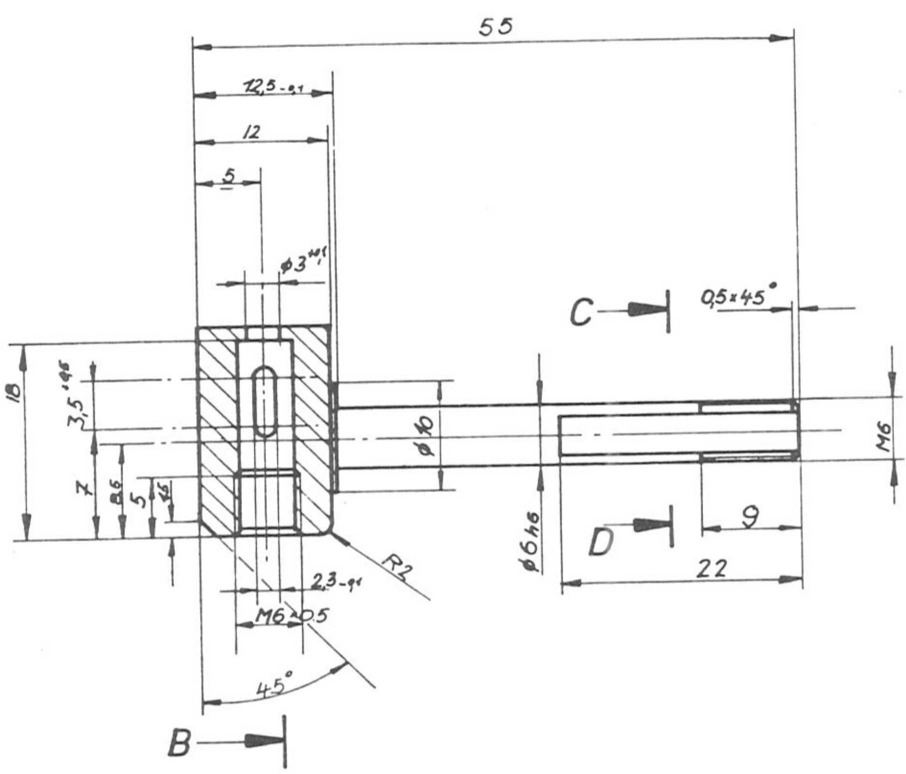

A-B

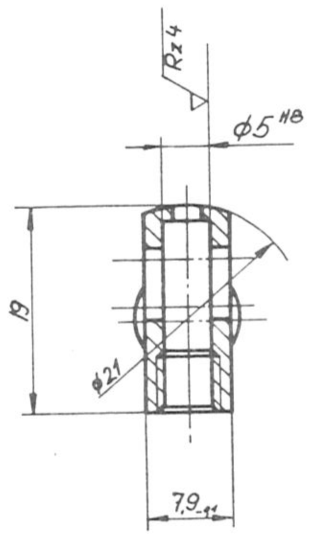

C-D

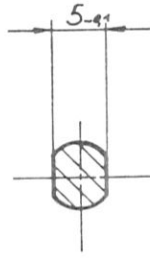

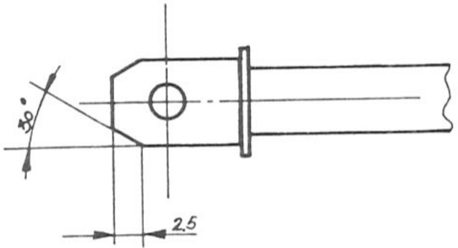

3D 1166 - 110a

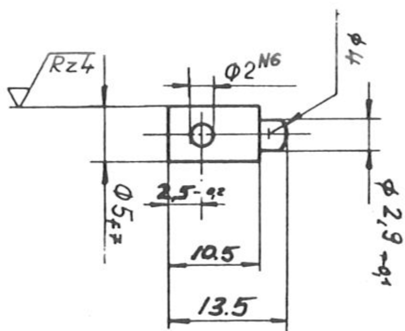
Rz4
Φ2 N6
Φ4
Φ5 f7
2,5 -0,2
10.5
13.5
Φ2,9 -0,1

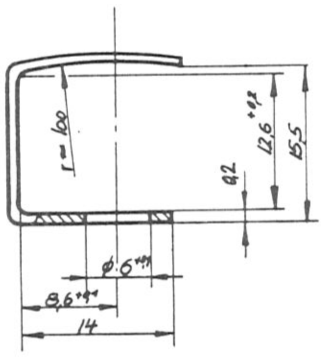
r ≈ 100
0,2
12,6 +0,2
15,5
⌀ 6 +0,1
8,6 +0,1
14

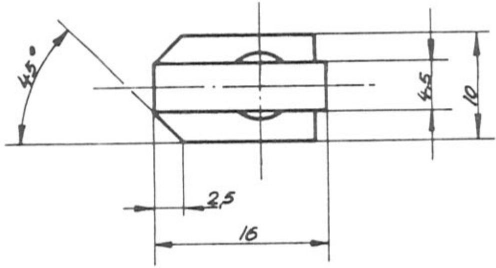
45°
4,5
10
2,5
16

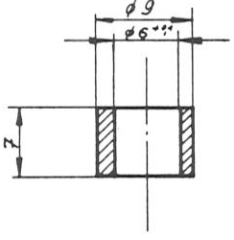
ø 9
ø 6 +0,1
7

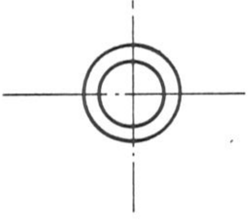

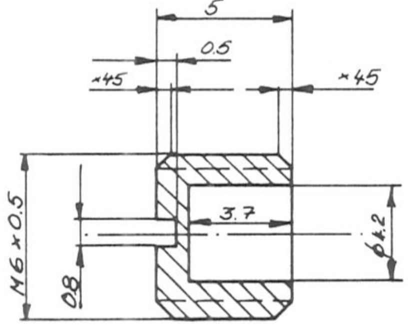

4D 1166-114